Conformational assessment of proteins by hydrogen exchange-mass spectrometry

By

H M Emranul Haque

Submitted to the graduate degree program in Chemistry Department and the Graduate Faculty of the University of Kansas in partial fulfillment of the requirements for the degree of Master of Science

.

Chair: David D. Weis, PhD.

Heather Desaire, PhD.

Krzysztof Kuczera, PhD.

Date Defended: 05/25/2021

The thesis committee for H M Emranul Haque certifies that this is
the approved version of the following thesis:

Conformational assessment of proteins by hydrogen exchange-mass spectrometry

Chair: David D. Weis, PhD.

Date Approved: 05/25/2021

Abstract

Hydrogen exchange-mass spectrometry (HX-MS) is a key analytical tool to study protein conformation and dynamics. In this technique, backbone amide hydrogens exchange with the heavy isotope of hydrogen (deuterium) in solution to give information related to the conformational state of protein. Hydrogen exchange by a protein can be measured by mass spectrometry and the results are often presented on a structural model of the protein. This technique has been used successfully to identify changes in protein conformational information at high resolution; here I have applied this technique to study two different proteins.

PsbO is an extrinsic membrane protein in photosystem II (PSII). PsbO has versatile functions in PSII. It is known that PsbO is released from PSII and contributes to the repair cycle of PSII following photodamage of PSII. The conformational states of bound and released PsbO are not the same. Previous studies found that the conformation of PsbO changes when it binds to PSII, but these studies did not reveal where exactly the structural changes were located. In this study I identified the locations of the structural changes of the released PsbO by using hydrogen exchange-mass spectrometry.

Ricin toxin subunit (RTA) has been under investigation for a long time as a potential vaccine against ricin intoxication. As a part of that effort, one approach is to engineer the RTA* antigen to stimulate production of neutralizing antibodies. In this study, I analyzed an engineered version of RTA* known as RTA*-SS. This engineered version has one extra disulfide linkage which was anticipated to stabilize one of the antibody binding hotspots known as α-helix B. I investigated the effect of mutation on the structure of RTA*-SS1 with special attention to the α-helix B site by hydrogen exchange-mass spectrometry. While HX-MS showed that statistically significant protection and deprotection in overall conformation due to insertion of disulfide linkage, I was

unable to determine the stability of α-helix B in RTA*-SS1, because faster HX was observed in that region and this faster HX exchange could be due to faster, slower or unchanged structural dynamics and faster chemical exchange.

Acknowledgments

First of all, I deeply appreciate my supervisor Prof. David D. Weis for his great support throughout my graduate studies journey. Prof. Weis was brave enough to accept me as the first transfer student in his lab. I am thankful to him for giving me all the training, projects, financial support, and for accepting my failures. I thank him for sharing his knowledge and expertise which greatly helped me to accomplish my research project work. The great part of joining the Weis lab was to learn the hydrogen exchange-mass spectrometry (HX-MS) technique from a prominent HX-MS researcher like Prof. Weis. Again, I thank him for giving me this learning opportunity, and for all the support.

I thank all the past and current group members of Weis lab for their support. I especially thank Dr. Tyler Hageman for giving me training during his busy schedule in thesis writing time.

I thank the Department of Chemistry, KU for allowing me to study here and supporting me all the time.

I appreciate my committee members, Prof. Heather Desaire and Prof. Krzysztof Kuczera for finding some time to serve on my thesis committee.

Finally, I thank my parents, my siblings, and my wife for all the support and the sacrifices they've made during my stay at KU.

I would like to dedicate this thesis to my parents and my elder brother who realized the importance of education and science.

Table of Contents

List of Figures

List of Tables

Chapter 1

Introduction

.

1.1 Hydrogen exchange mass spectrometry (HX-MS)

1.1.1 Brief history of HX-MS

Hydrogen exchange mass spectrometry (HX-MS) is a matured analytical technique for structural biology.[1, 2] HX-MS has become routine for studying higher-order structure of proteins, protein-protein interactions, protein-ligand interactions,[3] intrinsically disordered proteins,[4] allosteric effects in proteins,[5] folding dynamics of proteins [6] and epitope mapping[7] in academia and industry. This technique is highly reliable to identify the local structure or structural perturbation of proteins even when the change is subtle. Hydrogen exchange is now almost 70 years old. Hydrogen exchange in protein was first envisioned and initiated by Kaj Linderstrøm-Lang and his co-workers back in 1954 after the remarkable discovery of α-helix and β-sheet by Pauling-Corey-Branson. [8-10] The first hydrogen exchange experiment demonstrated hydrogen exchange in dried pork insulin and the amount of exchanged heavy isotope of hydrogens was determined by density measurement. That experiment paved the way for modern analytical tools in structural biology. Various detection methods such as infrared spectroscopy (IR),[11] ultraviolet spectroscopy (UV),[12] and nuclear magnetic resonance (NMR)[13] were employed in HX for structural biology. Hydrogen exchange measured by IR and UV are useful to get information with low resolution, but NMR is a higher resolution technique widely used for structural biology. In the 1970s and 1980s, NMR played a significant role as a detection method for hydrogen exchange. In the 1990s, the mass spectrometry based hydrogen exchange was started. In 1993, Zhongqi Zhang and David L. Smith introduced hydrogen exchange by using fragment based mass spectrometry technique to elucidate the rate of exchange in horse heart cytochrome c. This work was a major breakthrough for hydrogen exchange using mass spectrometry detection, and helped to advance that growing field into a matured and useful analytical technique.

HX-MS field has been evolved in the last 30 years with a lot of advancement. **Figure 1.1** shows the recent statistic of the HX-MS publication rate.[14] The publication rate of HX-MS focused on protein has been increased significantly in 2012 to 2020.

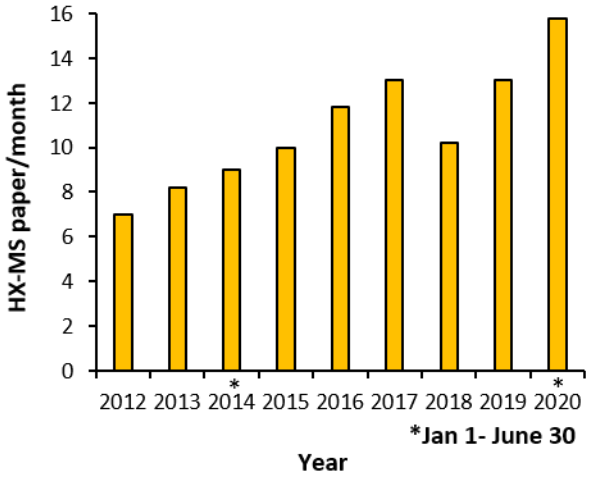

Figure 1.1. HX-MS publications per month published from 2012 to 2020 (figure adapted from Anal Chem 2021, 93 (1), 567-582.

1.1.2 Fundamentals of H/D exchange

All proteins are polypeptides composed of 20 different amino acids linked by covalent bonding in linear sequences. Backbone amide (N-H) linkages in α-helix or β-sheet are stabilized by hydrogen bonds. This backbone amide hydrogen bond provides structural information about a specific protein and its native state folding pattern. That backbone amide hydrogen is exchangeable with the surrounding solvent or gas with a heavier isotope of hydrogen (deuterium, tritium) in the millisecond to day's range. There are several other types of hydrogens that are covalently attached in protein structure: hydrogen with carbon, sulfur, nitrogen, oxygen (**Figure 1.2**). These hydrogens have different timescales of exchange. The most labile hydrogens that are located on side chains (O-H, S-H, N-H) exchange rapidly and monitoring this exchange by LC-MS is difficult. The hydrogens bonded to carbons do not exchange. MS monitors the exchange of amide hydrogens of

all amino acid residues except proline. Proline contains no amide hydrogen as a residue in protein structure.

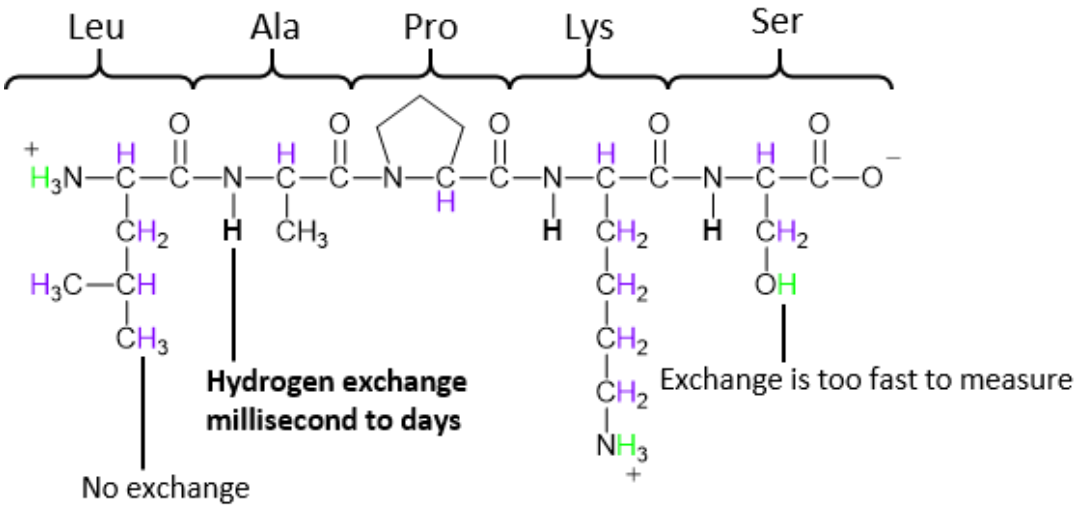

Figure 1.2. Unfolded penta-peptide to depict exchangeable hydrogen, black colored hydrogens are amide hydrogens that exchange hydrogen millisecond to days, purple colored hydrogens are non-exchangeable hydrogens, green colored hydrogens are fast exchangeable hydrogens.

Hydrogen exchange in backbone amide can be catalyzed by acid and base.[15] **Figure 1.3** shows the base- and acid-catalyzed hydrogen exchange mechanism. In a base-catalyzed hydrogen exchange reaction, a nucleophile (OH^- or OD^-) abstracts protium from the amide nitrogen and converts to amidate ion. In the next step, amidate nucleophile abstracts a deuterium from heavy water and the amidate becomes deuterated in the backbone amide nitrogen. Since the rate of base catalyzed HX is much faster in neutral pH, base catalyzed hydrogen exchange is predominant. Acid catalyzed hydrogen exchange takes place either as a protonation of amide nitrogen or a carbonyl oxygen. In acid-catalyzed HX through amide nitrogen site, nitrogen abstracts a deuterium from D_3O^+ and forms an intermediate which is subsequently deprotonated in the following step to deuterated amide. In acid catalyzed hydrogen exchange through an oxygen site, carbonyl oxygen

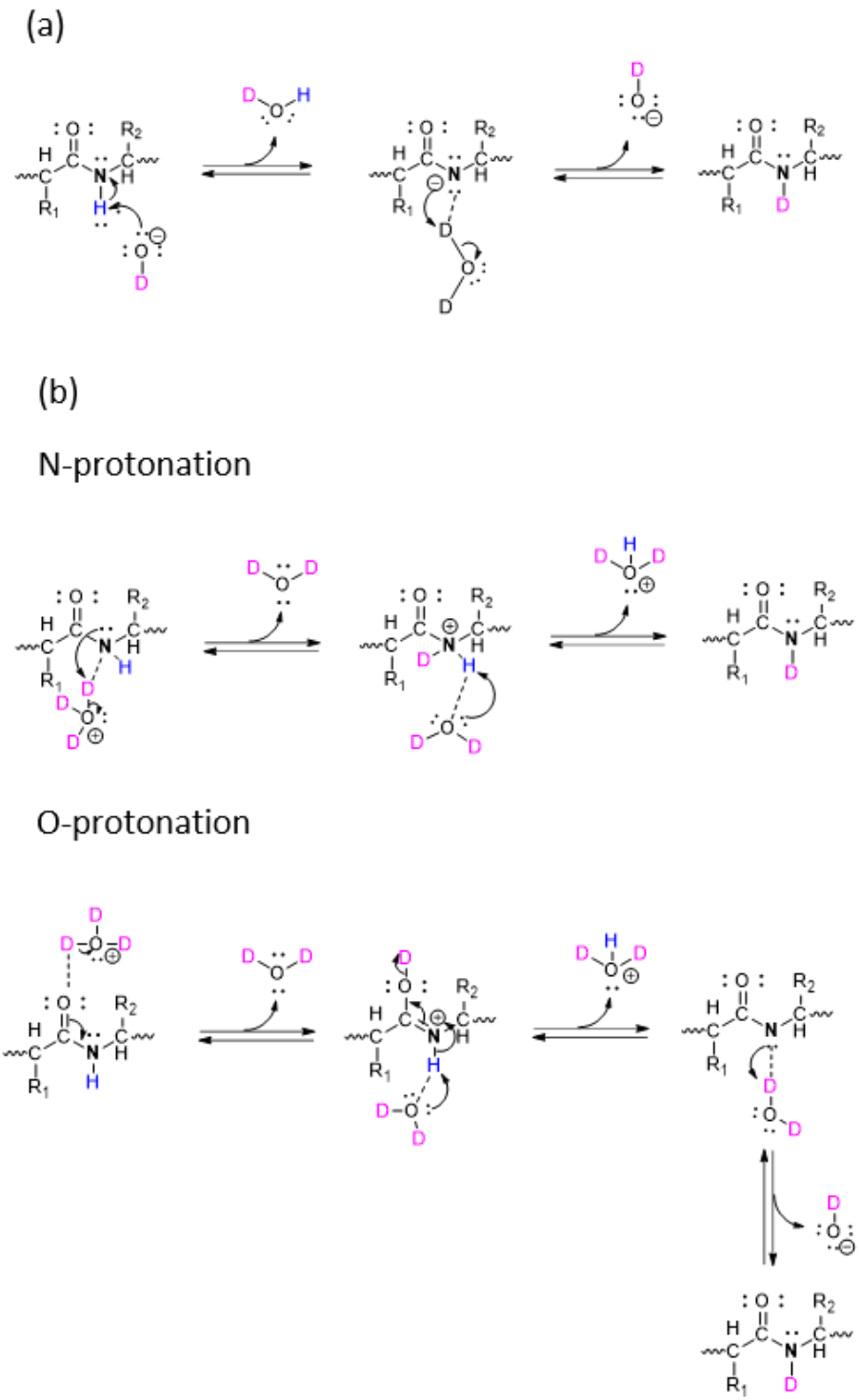

Figure 1.3. Hydrogen exchange mechanistic pathways by (a) base catalysis hydrogen exchange (b) acid catalysis (N-protonation and O-protonation). The figure was generated with Chemdraw professional.

gets protonated or deuterated, and subsequently acidifies amide nitrogen and forms imidic acid, and deuterates finally to deuterated amide. The acid catalyzed hydrogen exchange is still a matter of debate, because acid catalysis can occur by amide nitrogen or carbonyl oxygen or a combination of both.

Chemical exchange of hydrogen in protein primarily depends on pH and temperature. The secondary factors are solvent components, pressure, and inductive effects from neighboring residues. The pH dependence can be explained by the following equation:

$$k_{ch} = k_{intr,H}\,[H^+] + k_{intr,OH}\,[OH^-] + k_{intr,H_2O}\,[H_2O] \quad (1.1)$$

The measured intrinsic acid catalyzed rate constant $\left(k_{intr,H}\right)$ is 4.19×10^{-1} M^{-1} min^{-1}, base catalyzed rate constant $\left(k_{intr,OH}\right)$ is 1.67×10^{8} M^{-1} min^{-1} and water catalyzed rate constant $\left(k_{intr,H_2O}\right)$ is 4.19×10^{-4} M^{-1} min^{-1} for poly-DL-alanine.[16, 17] The base-catalyzed rate is higher than the acid catalyzed rate and water catalysis is negligible compared to the base catalyzed rate. **Figure 1.4** shows the plot of pH dependence of chemical hydrogen exchange rate constant(k_{ch}). The rate of acid- and base-catalyzed are nearly equal in the pH 2-3 range. The typical deuterium labeling conditions in HX are physiological pH (pH 7). At pH 2-3 range, the HX rate decreases in the four order of magnitude than the HX rate at pH 7. The hydrogen exchange rate increases 10-fold as 1.0 unit pH increases.

Temperature also affects the hydrogen exchange rate as increasing temperature increases exchange rate. Hydrogen exchange rate increases 10 fold with 0°C to 22°C increase of temperature. Increasing temperature increases the molecular motion, increases the collision frequency of proton donor and acceptor, and thus increases rate. Since pH and temperature affect hydrogen exchange rate, this two factors must be precisely controlled in the HX-MS experiment.

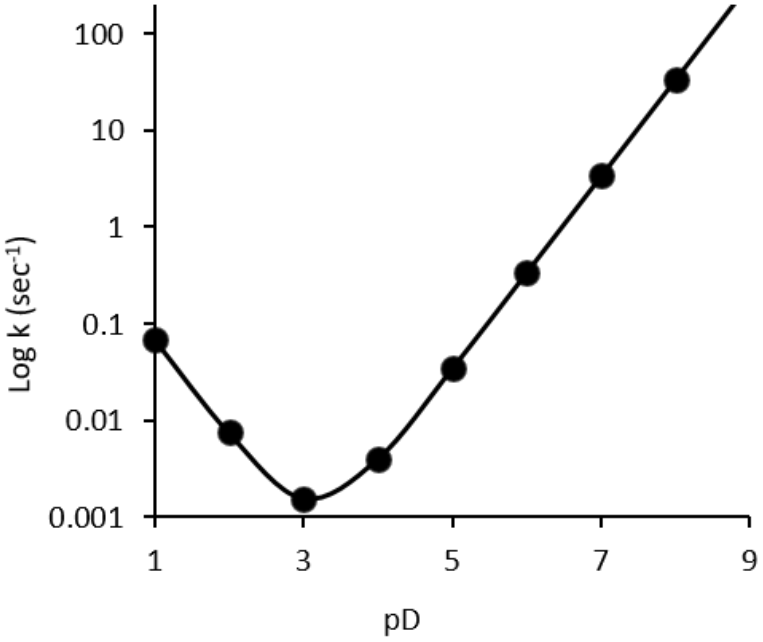

Figure 1. 4.Hydrogen exchange rate constant dependence on pD for poly-D,L-alanine at 20°C (*J. Am. Soc. Mass. Spectrom.***2018,** *29* (9), 1936-1939).

So combination of pH 2-3 and 0°C are used as HX quench condition because at this condition the exchange half-life is ~25 min which allow sufficient time for LC-MS to measure the HX kinetics and also the rate of back-exchange of HX is minimum. Back exchange is a phenomenon where deuterium labeled amide backbone in protein or peptide loses deuterium during liquid chromatographic separation in contact with mobile phase, because mobile phase contains water. To minimize the back exchange, maintaining a constant 0°C, pH 2-3 and short LC separation time is extremely important. Even in 0°C and pH 2-3, back exchange is still occurs and the amount of back exchange is considered when we calculate the deuterium uptake for a peptide (see equation 1.7). In addition to pH, temperature, residue side chain or neighboring group also affect hydrogen exchange rate. Hydrogen exchange of a peptide with isobutyl group in isoleucine was found 10-20 times slower by two isobutyl group in between alanine amide.[16]

Solution phase hydrogen exchange can be understood based on theoretical models such as the solvent penetration model and Linderstrøm-Lang model. The Linderstrøm-Lang model is based on the breathing motion of the protein combined with HX of an amide [18] and is the most widely-accepted model that helps to understand how hydrogen exchange occurs in a folded protein. Breathing motion of folded protein states that the intramolecular (N-H···C=O) hydrogen bond of protein transiently opens and closes. In HX results, when we see fast exchange that normally indicates solvent exposure and no hydrogen bonding. Also when we see slow exchange that indicates solvent protection and strong hydrogen bonding. The Linderstrøm-Lang model is shown in equation (1.2) to represent how HX works. Folded protein (N-H, closed) in the solution unfolds locally or globally (N-H, open) with a rate constant k_{op}, and refolds with rate constant k_{cl}. This temporal structural opening allows hydrogen exchange by the unprotected amide with rate constant k_{ch}.

$$N - H_{closed} \underset{k_{cl}}{\overset{k_{op}}{\rightleftarrows}} N - H_{open} \xrightarrow[D_2O]{k_{ch}} N - D_{open} \rightleftarrows N - D_{closed} \tag{1.2}$$

According to this model, in solution, protein structure can locally or globally unfolds and refolds, so the equation of (1.2) for hydrogen exchange rate (k_{HX}) of that protein can be represented by the following equation:

$$k_{HX} = \frac{k_{op} \times k_{ch}}{k_{op} + k_{cl} + k_{ch}} \tag{1.3}$$

In native condition, the refolding rate of a protein is much higher than the opening rate $k_{cl} \gg k_{op}$, so the equation (1.3) can be rewritten as,

$$k_{HX} = \frac{k_{op} \times k_{ch}}{k_{cl} + k_{ch}} \tag{1.4}$$

Based on the relative exchange rate of unfolding, refolding and chemical exchange, two extremes of HX kinetics referred as EX1 and EX2 are often observed. In the EX1 kinetic limit, $k_{ch} \gg k_{cl}$ and the equation (1.4) stands as,

$$k_{HX} = k_{op} \quad (1.5)$$

This hydrogen exchange rate is correlated with the protein unfolding rate. Under this category, since the protein refolding rate is slower than the chemical exchange rate, it gives enough time for the chemical exchange in all positions. As a result of that, we see bimodal isotopic distribution in the mass spectrum.[19] In that bimodal distribution, the higher mass envelope indicates of full exchange and the lower mass envelope indicates no exchange. In EX2 kinetic limit, $k_{ch} \ll k_{cl}$ and the equation (1.4) stands as,

$$k_{HX} = \frac{k_{op}}{k_{cl}} \times k_{ch} = K_{op} \times k_{ch} \quad (1.6)$$

($K_{op} = \frac{k_{op}}{k_{cl}}$, equilibrium constant of protein unfolding)

The hydrogen exchange rate is correlated to the ratio of protein unfolding to refolding and intrinsic chemical exchange. Under this condition, the protein refolding rate is much faster than the intrinsic chemical exchange rate and we see unimodal isotopic distribution in the mass spectrum. We see unimodal isotopic distribution because the protein undergoes multiple unfoldings and that gradually deuterates the amides. In HX-MS, EX2 kinetics are mostly seen, whereas, EX1 is rare. Peptides exhibiting EX1 kinetics are challenging to analyze because of bimodal isotopic profile (**see chapter-2, section 2.3.2**).

1.1.3 Workflow

Figure 1.5 shows the experimental workflow of hydrogen exchange. In a typical HX-MS experiment, a protein of interest is diluted in buffer prepared in heavy water (D_2O), typically pH 6-8. Dilution depends on the experimental design, but typically dilution can be ~4-20 fold. This

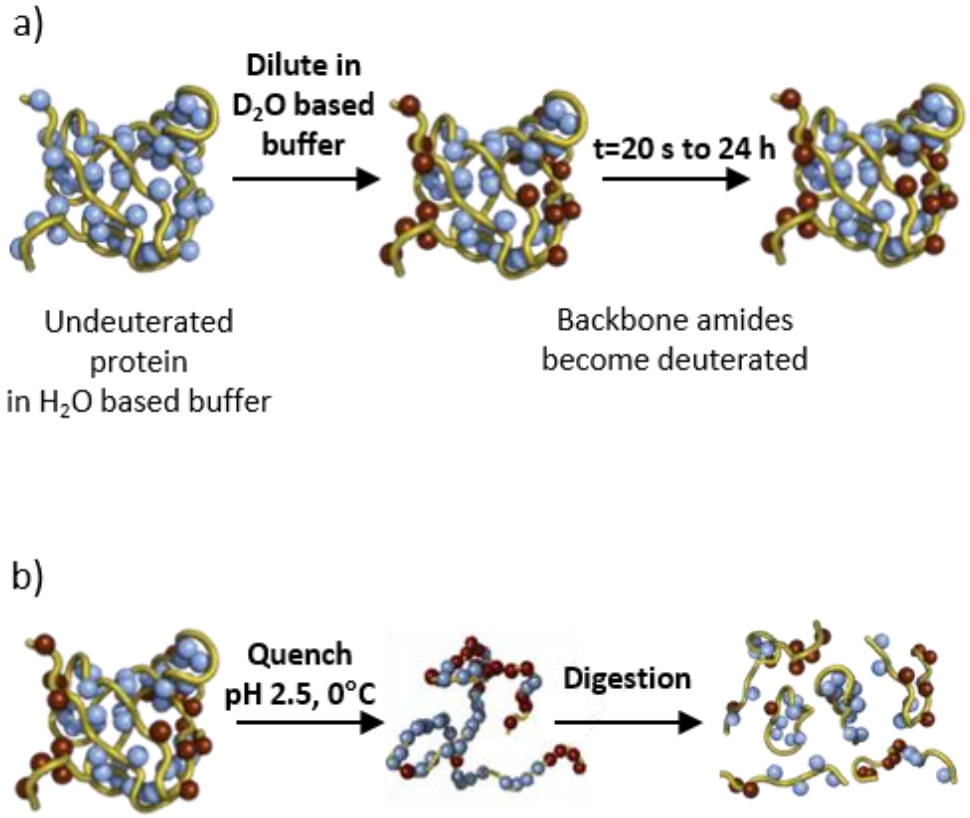

Figure 1. 5. HX-MS working scheme (a) labeling steps of undeuterated protein to deuteration (b) deuterated protein quench and digestion.

step is known as labeling (**Figure. 1.5a**). In the labeling step backbone amide protium exchanges with deuterium at different time intervals (**Figure.1.5a**). Labeling reaction of protein is stopped by the quenching solution at pH ~2-3 and 0°C to lower the HX rate significantly (**see section 1.1.2**). Quench solution is then inject to the LC system for digestion (**Figure. 1.5b**). Typically protein is

digested by an acid protease like pepsin. Peptides are separated by reversed-phase liquid chromatography and analyzed by mass spectrometry.

1.1.4 Analysis of HX-MS Data

Figure 1.6 shows the data analysis scheme of HX-MS from total ion chromatogram (TIC) to HX uptake plot. Once the mass spectrometer acquires the data, it is analyzed further by data analysis software such as, HDExaminer, DynamX, HDX Workbench, Mass Spec Studio. The working principle of all of these software's are same. First of all, peptide mapping of an undetuerated protein is done with MSMS to identify the peptides and find out the retention time to make a peptide data base. Data analysis software uses the data base to extract spectra of all peptides at correct retention time. Data analysis software then extracts the spectra of deuterated peptides using retention time and mass of the peptides. After that, data analysis software calculates the centroid masses of the peptides at each labeling time points. The deuterium uptake is determined by the centroid mass of the undeuterated peptide and deuteration at each labeling time points. The absolute deuterium uptake is calculated by equation 1.7 correcting for back-exchange in HX-MS.

$$D = \left(\frac{m - m_{0\%}}{m_{100\%} - m_{0\%}}\right) N \qquad (1.7)$$

D is the deuterium uptake corrected for back-exchange, m is the average mass of the peptide at labeling time point, $m_{0\%}$ is the average mass of the peptide at undeuterated control, $m_{100\%}$ is the average mass of the fully deuterated control, and N is the number of amides in the peptide. In HX-MS, typically two protein states are compared like protein in free state with ligand-bound states, so the back exchange remains constant throughout the same experimental for both protein states. After the mass calculation step is done, a plot of deuterium uptake with labeling time points is displayed known as an uptake plot. At the same time, the HX differences of all

peptides at all labeling time points are often tested for significance using different kinds of test (as an example, HDExaminer applies hybrid statistical significance testing[20] and data presented as a volcano plot).These data are usually mapped onto the crystal structure of that protein to display the HX results.

1.1.5 Advantages

HX-MS has been successfully established as a valuable technique in structural biology which can complements other structural biological techniques like nuclear magnetic resonance (NMR), electron microscopy (EM), native mass spectrometry, molecular dynamics, and X-ray crystallography. HX-MS consumes small sample amount of sample (<1 mg) and is capable of analyzing protein of any size. Unlike X-ray technique, HX-MS does not need crystallization. In HX-MS, we get solution dynamic behavior of protein whereas, we get static view of protein in the crystallized state. Technological advancement, like robots, reduced the labor to prepare a sample.

1.1.6 Limitations

HX-MS works best when the structure of that protein is available to put the data onto. HX-MS data cannot be used to solve protein structure like X-ray crystallography data or NMR data. The digestion step is extremely important to HX-MS. When the protein doesn't digest well, peptide level HX-MS cannot proceed. There are a limited number of acid proteases available, so options are limited for choosing acid protease. Resolution of HX-MS still needs to be improved as it provides on average 10-15 residues level resolution now. When peptides are long, HX data are not useful to extract structural information. When peptide coverage is limited, HX is not useful to get the structural information of that particular region. Data analysis of HX-MS has improved a lot from days to hours, but still it needs to be improved more to get the final results promptly.

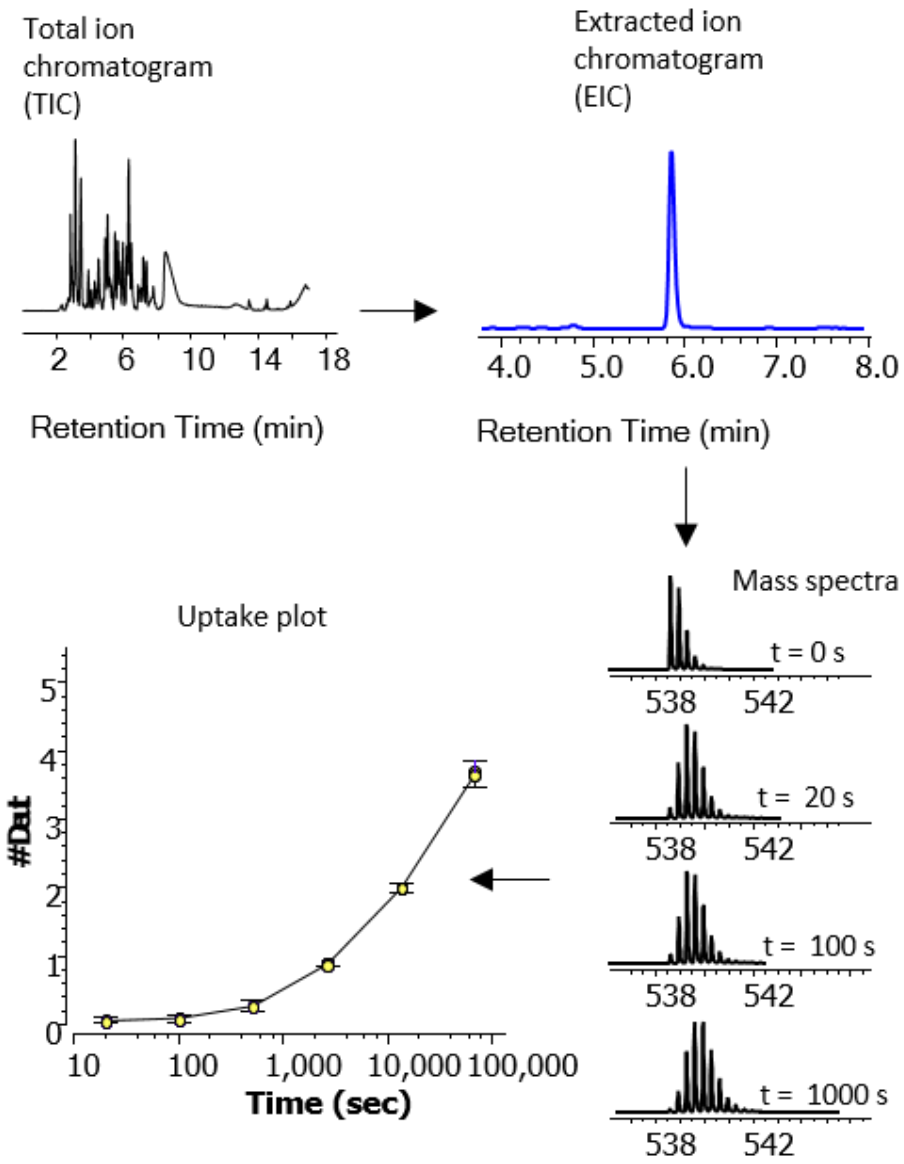

Figure 1.6. HX-MS data analysis scheme.

1.2 LC-MS analysis of peptides

1.2.1 Reversed-phase liquid chromatography

In high performance liquid chromatography (HPLC), reversed phase liquid chromatography (RPLC) is a popular choice for separating peptide molecules because of its high resolution. This separation technique is widely used in proteomics. RPLC, first developed by Hovarth and his co-workers, separates molecules based on hydrophobicity. [21] [22, 23] In RPLC, the stationary phase is based on hydrophobic (C18, C8, C3, phenyl etc) bonded to porous silica that can separate biomolecules. Mobile phase is water-miscible organic solvent like acetonitrile, methanol, or isopropanol used as gradient elution. Gradient elution is the changing of the composition of the mobile phase, typically increasing the fraction of organic solvent with time (e.g., 5-95%) to separate molecules based on hydrophobicity. So, in a gradient elution in RPLC, more polar solute is retained less strongly elute first and more hydrophobic larger solute retained more so elute later.

1.2.2 Mass spectrometry: electrospray ionization (ESI) method

Electrospray ionization (ESI) is a widely used ionization method for biomolecule analysis because it is a soft ionization technique. ESI was first developed In 1988, by John Fenn and co-workers for analyzing biomolecules without breaking them apart.[24] ESI is considered as soft ionization technique because it doesn't break any covalent bonds during ionization. In this technique liquid molecules are converted into gas-phase cationic or anionic species before analysis by mass analyzer. After the sample separated by LC, the liquid sample is sprayed through a metal nebulizer that is held at 3-6 kV potential and also in heated nitrogen gas. The sample solution when sprayed, it forms a Tylor cone before going into the mass spectrometer inlet as shown **Figure 1.7a**.

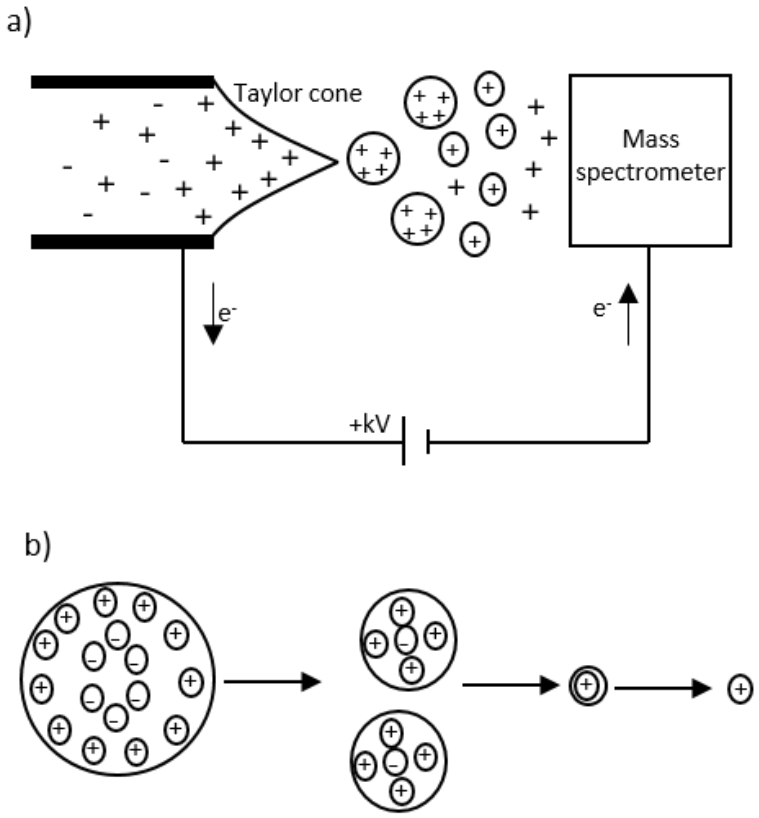

Figure 1. 7. (a) Electrospray ionization source (b) Scheme of forming analyte ion from charged droplet.

The charged droplets shrinks because of the desolvation process by heated gas over the larger droplet and smaller droplets undergo this process again. ESI has several cycles of evaporation and explosion. **Figure 1.7b** shows the scheme of the conversion from the larger to tiny droplet. The shrunken larger droplet explodes when the Columbic repulsion forces take over the cohesive forces of the larger droplet. The charge-charge repulsion creates a stream of charged ions which then moves to the inlet of mass spectrometer (**Fig.1.7b**).

1.2.3 Mass spectrometry: Time-of-Flight (TOF) Mass analyzer

Time of flight (TOF) mass analyzer measures the time that an ion takes to travel in flight tube to the detector. TOF is a popular mass analyzer often coupled with another mass analyzer like a quadrupole. In 1946, Stephens originated the idea of TOF which was later commercialized as a

linear TOF mass spectrometer based on the article by Wiley and McLaren.[25, 26] The salient point of TOF is ions with lighter m/z travel faster than the heavier m/z ion before detection. **Figure 1.8** shows the time of flight tube contains its parts like ion pulser, ion mirror, and ion detector. When the sample is ionized in the ionization chamber, it travels through a quadruple mass analyzer, collision cell, transfer optics, and then into a flight tube for detection. The mass/charge (m/z) ratio of an ion can be derived from the time it takes a packet of ions to travel from ion pulser to detector. The following equation shows the relations of the time to the m/z :

If a ion with mass (m), total charge (q=ze) accelerated by potential V_s, then the electric potential energy is converted to the kinetic energy,

$$\text{Kinetic energy, } \frac{1}{2}mv^2 = zeV_s \tag{1.8}$$

From equation (1.8), velocity of the ion,

$$v = \sqrt{\frac{2zeV_s}{m}} \tag{1.9}$$

If the time (t) required for an ion to travel a flight tube length (L) with velocity (v),

$$t = \frac{L}{v} \tag{1.10}$$

Then from equation (1.9) and (1.10),

$$t^2 = \frac{m}{z}\left(\frac{L^2}{2eVs}\right) \tag{1.11}$$

$$\frac{m}{z} = t^2\left(\frac{2eV_s}{L^2}\right)$$

$$\frac{m}{z} \propto t^2 \tag{1.12}$$

While other terms (fight tube length, potential) are constant (equation 1.12)), the m/z is proportional to the time squared. So, the lighter m/z requires less time than the heavier mass for the detection.

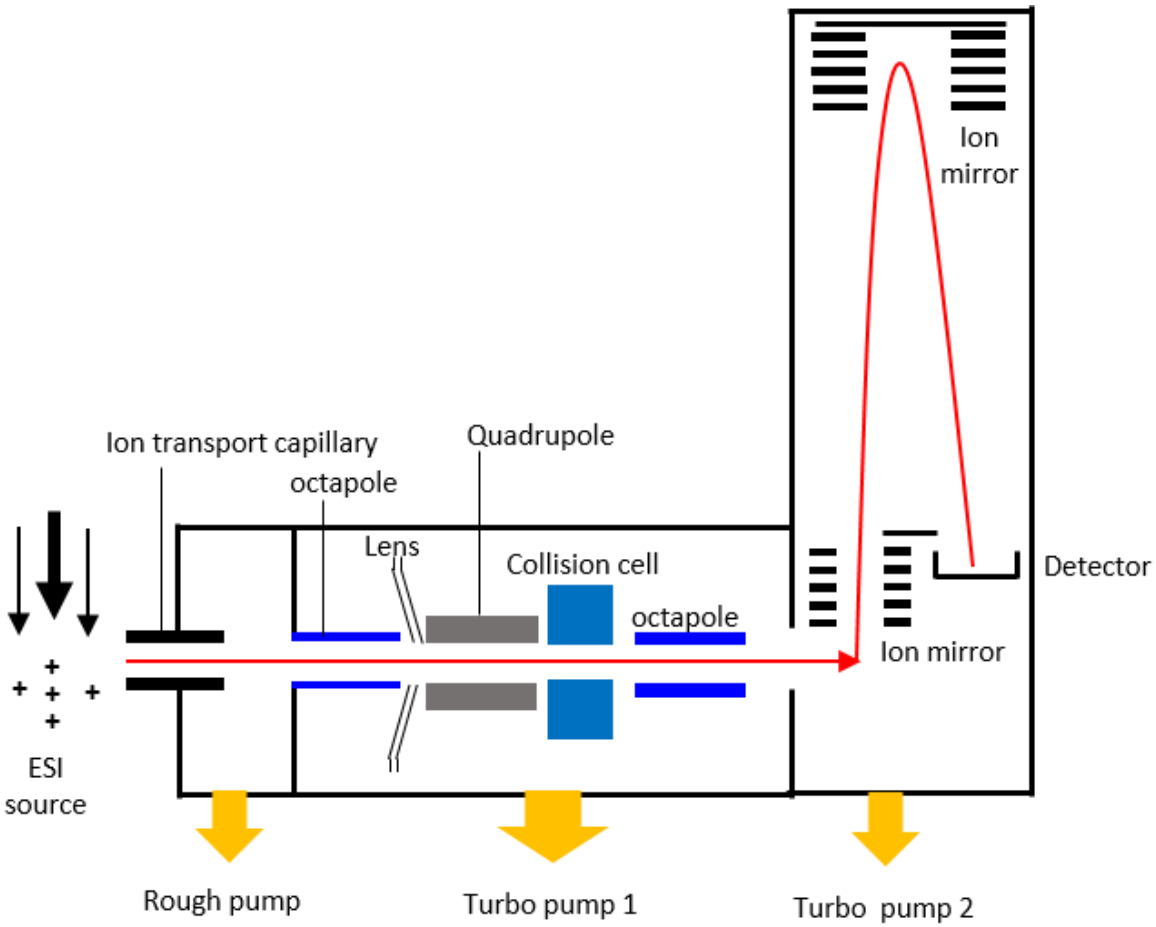

Figure 1. 8. Schematic diagram of QTOF (adapted from *Agilent 6200 series TOF and 6500 series QTOF LC-MS System, Agilent Technologies, 2015*).

1.2.4 Mass spectrometry: Tandem mass spectrometry (MSMS) for peptide identification

Tandem mass spectrometry is a combination of two mass analyzers. Tandem mass spectrometry (MSMS) is s used to identify and confirm a sequence of the protein and peptides. In this technique, the precursor (the ion that is detected by first mass analyzer, undergoes fragmentation) is analyzed by fragmentation and that brings change to the mass or charge of the precursor, and those ions are called product ions. Tandem mass spectrometry starts with selecting the precursor ion using the first mass analyzer, and then precursor further undergoes fragmentation before the fragments are analyzed by the second mass analyzer. There are the different techniques

for in tandem mass spectrometry fragmenting the precursor ion including collision-induced dissociation, electron capture dissociation, and electron transfer dissociation. One of the most popular ones is the collision-induced dissociation fragmentation (CID) technique. In this technique, the selected precursor ion from the first mass analyzer collides with neutral gas molecules (He, Ar, N_2) to get fragmented. CID has the specificity of the fragmentation location. **Figure 1.9a** shows the location of the fragmentation in the CID technique. In CID, fragmentation usually occurs in amide linkage (-CO-NH) to produce b and y products ions. The mechanism of the fragmentation can be understood by the mobile proton model (MPM).[27-29] In MPM, the proton from the N-terminal or any basic residues like lysine, arginine transfer to the carbonyl oxygen or amide nitrogen that initiates the cleavage of that amide bond called charge directed fragmentation.

Tandem mass spectrometry (MSMS) select the precursor ion by first mass analyzer and then that precursor ion produces products ions which are analyzed by second mass analyzer. **Figure 1.9b** shows the example of how MSMS analysis of a peptide works. After isolating a precursor m/z: 462.26 by first mass analyzer, it transmit to the collision cell and here it fragments in to b_3, y_2, y_5, b_5 etc products ions and analyzed by second mass analyzer. The mass of the product ions (b_3, y_2, y_5, b_5 etc) matches with the database by data analysis software. The important point is, two different peptides with same precursor mass will have different fragments. Selection of precursor ion and convert that to product ions confirm a specific peptide sequences.

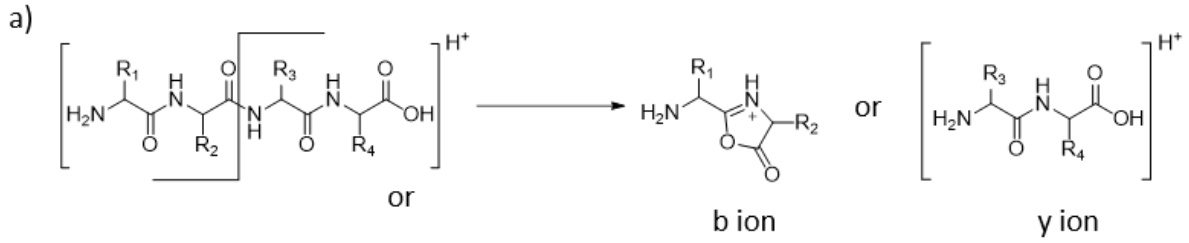

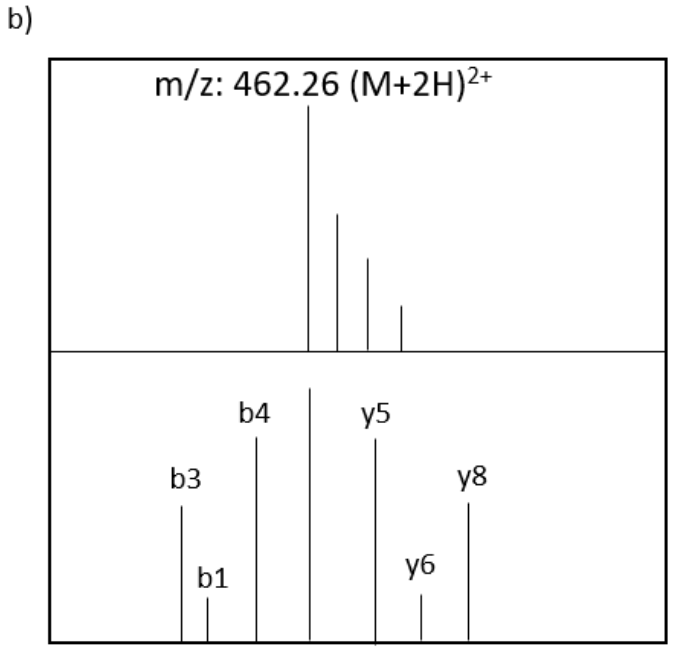

AGAYTISKL

b1 A GAYTISKL y8

b3 AGA YTISKL y6

b4 AGAY TISKL y5

Figure 1. 9. (a) Fragmentation of a dipeptide to product ions (b,y) by CID, (b) example of product ions from a precursor m/z, 462.26 $(M+2H)^{2+}$.

1.3 References

1. Jensen P.F., R. K. D., Hydrogen exchange: A sensitive analytical window into protein conformation and dynamics. In *Hydrogen exchange mass spectrometry of proteins:Fundamentals, Methods, and Applications*, Weis, D. D., Ed. John Wiley & Sons: 2016; pp 1-26.

2. Weis, D. D., Hydrogen exchange mass spectrometry of proteins: fundamentals, methods, and applications. John Wiley & Sons: 2016.

3. Chalmers, M. J.; Busby, S. A.; Pascal, B. D.; West, G. M.; Griffin, P. R., Differential hydrogen/deuterium exchange mass spectrometry analysis of protein–ligand interactions. *Expert review of proteomics* **2011,** *8* (1), 43-59.

4. Balasubramaniam, D.; Komives, E. A., Hydrogen-exchange mass spectrometry for the study of intrinsic disorder in proteins. *Biochimica et Biophysica Acta (BBA)-Proteins and Proteomics* **2013,** *1834* (6), 1202-1209.

5. Englander, J. J.; Del Mar, C.; Li, W.; Englander, S. W.; Kim, J. S.; Stranz, D. D.; Hamuro, Y.; Woods, V. L., Protein structure change studied by hydrogen-deuterium exchange, functional labeling, and mass spectrometry. *Proceedings of the National Academy of Sciences* **2003,** *100* (12), 7057-7062.

6. Englander, S. W.; Mayne, L., The nature of protein folding pathways. *Proc Natl Acad Sci U S A* **2014,** *111* (45), 15873-80.

7. Deng, B.; Lento, C.; Wilson, D. J., Hydrogen deuterium exchange mass spectrometry in biopharmaceutical discovery and development - A review. *Anal Chim Acta* **2016,** *940*, 8-20.

8. Hvidt, A.; Nielsen, S. O., Hydrogen exchange in proteins. In *Advances in protein chemistry*, Elsevier: 1966; Vol. 21, pp 287-386.

9. Hvidt, A.; Linderstrøm-Lang, K., Exchange of hydrogen atoms in insulin with deuterium atoms in aqueous solutions. *Biochimica et biophysica acta* **1954,** *14* (4), 574.

10. Eisenberg, D., The discovery of the α-helix and β-sheet, the principal structural features of proteins. *Proceedings of the National Academy of Sciences* **2003,** *100* (20), 11207-11210.

11. Osborne, H. B.; Nabedryk-Viala, E., The Conformation of Membrane-Bound and Detergent-Solubilised Bovine Rhodopsin: A Comparative Hydrogen-Isotope Exchange Study. *European journal of biochemistry* **1978,** *89* (1), 81-88.

12. Englander, J. J.; Calhoun, D.; Englander, S. W., Measurement and calibration of peptide group hydrogen-deuterium exchange by ultraviolet spectrophotometry. *Analytical biochemistry* **1979,** *92* (2), 517-524.

13. Englander, S. W.; Mayne, L., Protein folding studied using hydrogen-exchange labeling and two-dimensional NMR. *Annual review of biophysics and biomolecular structure* **1992,** *21* (1), 243-265.

14. Engen, J. R.; Botzanowski, T.; Peterle, D.; Georgescauld, F.; Wales, T. E., Developments in Hydrogen/Deuterium Exchange Mass Spectrometry. *Anal Chem* **2021,** *93* (1), 567-582.

15. Perrin, C. L., Proton exchange in amides: Surprises from simple systems. *Accounts of Chemical Research* **1989,** *22* (8), 268-275.

16. Bai, Y.; Milne, J. S.; Mayne, L.; Englander, S. W., Primary structure effects on peptide group hydrogen exchange. *Proteins: Structure, Function, and Bioinformatics* **1993,** *17* (1), 75-86.

17. Nguyen, D.; Mayne, L.; Phillips, M. C.; Walter Englander, S., Reference parameters for protein hydrogen exchange rates. *Journal of The American Society for Mass Spectrometry* **2018,** *29* (9), 1936-1939.

18. Englander, S.; Mayne, L.; Bai, Y.; Sosnick, T., Hydrogen exchange: the modern legacy of Linderstrøm-Lang. *Protein science* **1997,** *6* (5), 1101-1109.

19. Engen, J. R.; Smithgall, T. E.; Gmeiner, W. H.; Smith, D. L., Identification and localization of slow, natural, cooperative unfolding in the hematopoietic cell kinase SH3 domain by amide hydrogen exchange and mass spectrometry. *Biochemistry* **1997,** *36* (47), 14384-14391.

20. Hageman, T. S.; Weis, D. D., Reliable Identification of Significant Differences in Differential Hydrogen Exchange-Mass Spectrometry Measurements Using a Hybrid Significance Testing Approach. *Anal Chem* **2019,** *91* (13), 8008-8016.

21. Horvath, C.; Melander, W.; Molnar, I., Solvophobic interactions in liquid chromatography with nonpolar stationary phases. *Journal of chromatography. A* **1976,** *125* (1), 129-156.

22. Horváth, C.; Melander, W.; Molnar, I., Liquid chromatography of ionogenic substances with nonpolar stationary phases. *Analytical Chemistry* **1977,** *49* (1), 142-154.

23. Horvath, C.; Melander, W., Liquid chromatography with hydrocarbonaceous bonded phases; theory and practice of reversed phase chromatography. *Journal of Chromatographic Science* **1977,** *15* (9), 393-404.

24. Fenn, J. B.; Mann, M.; Meng, C. K.; Wong, S. F.; Whitehouse, C. M., Electrospray ionization for mass spectrometry of large biomolecules. *Science (New York, N.Y.)* **1989,** *246* (4926), 64-71.

25. Stephens, W., A Pulsed Mass Spectrometer with Time Disaersion. *Phys. Rev.* **1946,** *69*, 691.

26. Wiley, W.; McLaren, I. H., Time-of-flight mass spectrometer with improved resolution. *Review of scientific instruments* **1955,** *26* (12), 1150-1157.

27. Summerfield, S. G.; Whiting, A.; Gaskell, S. J., Intra-ionic interactions in electrosprayed peptide ions. *International Journal of Mass Spectrometry and Ion Processes* **1997,** *162* (1-3), 149-161.

28. Dongré, A. R.; Jones, J. L.; Somogyi, Á.; Wysocki, V. H., Influence of peptide composition, gas-phase basicity, and chemical modification on fragmentation efficiency: Evidence for the mobile proton model. *Journal of the American Chemical Society* **1996,** *118* (35), 8365-8374.

29. Wysocki, V. H.; Tsaprailis, G.; Smith, L. L.; Breci, L. A., Mobile and localized protons: a framework for understanding peptide dissociation. *Journal of Mass Spectrometry* **2000,** *35* (12), 1399-1406.

Chapter 2

Templating by photosystem II induces persistent structure in PsbO as revealed by hydrogen exchange-mass spectrometry (HX-MS)

2.1 Introduction

Photosynthesis is the conversion of solar energy into chemical energy using natural tools like plant leaves, cyanobacterium and algae. In plants, chloroplasts conduct a complicated chemical process to generate oxygen from water using solar energy. This photosynthetic process initiates with photosystem II (PSII) in the thylakoid membrane. PSII is a multimeric membrane protein complex system that splits water molecules into protons, electrons, and molecular oxygen. The epicenter for this process in PSII is known as the oxygen-evolving center (OEC, or manganese center). Spinach PSII monomeric unit is comprised of four large (D1, D2, CP43, and CP47) intrinsic subunits, twelve low molecular weight membrane-spanning intrinsic subunits, and four extrinsic subunits (PsbO, PsbP, PsbQ, and PsbTn).[1] PsbO is one of the extrinsic subunits of PSII located on the lumenal site of the thylakoid membrane from the PSII, close to the OEC. PsbO is a prominent subunit because of its close proximity to the manganese center, its function, and structure.

PsbO is known for its versatile functions in PSII including stabilization of manganese clusters, retention of calcium and chloride ion concentration in OEC,[2] oxygen evolution,[3] proton transfer,[4, 5] and protecting PSII during photo-damage and repair from photodamage.[6-8] PSII can become damaged due to abiotic stress and PSII can also repair itself naturally. In a dynamic process of repair following abiotic damage, the PsbO subunit is released from PSII. Literature suggests about 50% of the total pool of PsbO are soluble (released) and that these free PsbO stay in thylakoid lumen where they might maintain homeostasis.[9] To naturally regenerate *de novo* PSII, photodamaged PSII needs to be partially dissembled, at that time, free PsbO maintains the interaction between photodamaged intrinsic subunits D1 and CP43. The extended structure of PsbO also protects D1 from reactive oxygenic species (ROS).[10] According to the current state of

knowledge, a holistic picture of photodamage repair and the critical contribution of PsbO to PSII protection and repair are yet to be fully understood. To elucidate the role of free PsbO in PSII repair, it is important to understand the conformational state of free PsbO in the thylakoid lumen and the specific part of PsbO structure that participates in the repair process. In this work, we have investigated the structural part of PsbO when PsbO is released from PSII, which can provide valuable insight into the function of PsbO related to photodamage and repair and other related functions.

Released PsbO has been classified as a natively unfolded (or intrinsically disordered) protein.[2, 11-13] PsbO has been classified as a natively unfolded protein because its resistance to thermal inactivation, its high random coil and turn content (4-75% IR, 45-55% CD), and its low pI (5.2) are comparable to other natively unfolded proteins.[11] PsbO can be extracted from intact PSII by treatment with alkaline-tris, $CaCl_2$, $MgCl_2$, and urea-NaCl, and then subsequently reconstituted into PSII to restore PSII function.[14-18] IR spectroscopic studies show that PSII acts as a template for PsbO, because PsbO secondary structure content increases 30-40% (random coil percentage decreases and β-sheet percentage increases) upon binding to PSII. Structural perturbation occurs reversibly between isolated PsbO to PsbO bound with PSII. A template effect is seen because of the hydrogen bonding difference between released PsbO and recombinant PsbO. In *E. coli*-derived recombinant PsbO there was also an increase in hydrogen bonding in PsbO upon binding to PSII.[19] Based on these studies, the solution structure of released PsbO is classified as metastable or being in a shallow energy minimum. Interestingly, small-angle X-ray scattering measurements indicate that the size and shape of PsbO does not change from solution to bound form. The secondary structural difference in PsbO before and after the reconstitution with PSII gives evidence that PSII acts as a template for natively unfolded PsbO.

All the aforementioned studies of PsbO employed low resolution IR spectroscopy, CD, which are sensitive to detect the secondary structure on the global level, but these techniques cannot provide the location of the structural changes. Current understanding about templated folding or binding induced folding of natively unfolded PsbO is very limited. Here, we examine the template effect of PSII on PsbO released from spinach PSII measured using a higher-resolution technique, hydrogen exchange-mass spectrometry (HX-MS). To elucidate the template effect, we identified conformational differences between released PsbO (extracted from spinach PSII) and *E. coli* derived recombinant PsbO. This chapter discusses HX-MS results in the context of the template effect of PSII on PsbO. The novel finding of our work are the specific locations of the template effect on PsbO released from PSII, which has not been revealed by previous low-resolution techniques.

2.2 Material and Methods

2.2.1 Materials

PsbO samples were a gift from Prof. Bridgette Barry (Georgia Institute of Technology, Atlanta, GA, USA). Samples were received in phosphate buffer (20 mM phosphate, 100 mM NaCl, pH 6.5) and used as received. Released PsbO was extracted from spinach PSII by $CaCl_2$ treatment,[15] and recombinant PsbO was expressed in *E. coli*. [20-22] MS analysis showed that the mass of released and recombinant PsbO matched to the theoretical masses within ±0.2 Da (**Appendix A, Figure 2.A-1**), indicating that the measured masses of released and recombinant PsbO are consistent with the amino acid sequences, including one disulfide bond. In recombinant PsbO, we have found a low abundance peak in addition to the major product peak. The mass of low abundance peak is 26022.5 Da (**Appendix A, Figure 2.A-1b**). The mass difference between the recombinant PsbO (26663.25 Da) and low mass peak of PsbO (26022.50) is 640.75 Da

consistent with the removal of (-EGGKRL-) residues from with mass 640.71 Da. This observation suggests that the low mass peak is a population of internally truncated recombinant PsbO which has the same amino acid sequence as recombinant PsbO, except (-EGGKRL-) residues. The abundance of truncated recombinant PsbO is ~6 times lower than the major peak. For structural comparison of released and recombinant PsbO, the presence of the truncated PsbO in the recombinant PsbO sample is not an issue because the truncation is located in the N-terminal loop region and thus absence of the truncated region is unlikely to alter the conformation or dynamics of the rest of PsbO.

2.2.2 HX-MS Measurements

Released PsbO (10.5 µM) and recombinant PsbO (17 µM) were collected from -80°C storage and thawed. The thawed recombinant PsbO sample was diluted to 10.5 µM by adding protein buffer (20 mM phosphate, 100 mM NaCl in water, pH 6.5). In an automated HX system deuterium labelling was conducted by HDX PAL robot (LEAP Technologies, Carrboro, North Carolina). During the deuterium labelling, 4 µL of each sample was diluted in 36 µL of protein buffer in D_2O (20 mM phosphate, 100 mM NaCl in D_2O, pD 6.5, pD was corrected for the isotopic effect[23]). In the following step, hydrogen exchange was conducted for 20, 100, 1000, 10000, 36000 and 72000 s with three replicates at 25°C. After labelling, 35 µL sample was quenched by 35 µL of quench buffer (200 mM glycine and 0.5 M TCEP•HCl at pH 2.5) at 0°C.

To find out the maximum deuterium uptake by each peptides, we conducted a maximal deuterium uptake experiment separately. Recombinant PsbO was labelled with buffer (20 mM phosphate, 100 mM NaCl with 6.67 M D_4-urea (98%), 0.5 M TCEP•HCl dissolved in D_2O (pH 6.1, pD 6.5) for one hour at 25°C. Labelled PsbO was quenched by 200 mM glycine, pH 2.50.

2.2.3 LC-MS analysis

Peptides from recombinant PsbO were generated by digesting on an immobilized pepsin column that was prepared in house.[24] Peptides were separated on an Agilent 1260 series (Santa Clara, CA) LC system. All peptides were trapped and desalted by C-8 (Zorbax 300SB C8, 2.1 x 12.5 mm, 5 µm particles) and separated by a C-18 column (Zorbax 300SB 2.1 × 50 mm, 3.5 µm particle diameter, Agilent, Santa Clara, CA). Mobile phase A was 0.1% formic acid in water, and B was 0.1% formic acid in acetonitrile (gradient 15%-40%B for 10 minutes) with flow rate 200 µL/min. For the peptic peptide mapping, all the peptides were assigned by MSMS using collision induced dissociation (CID) fragmentation technique. Agilent MassHunter Qualitative Analysis with BioConfirm (version B.07.00) software was used for the analysis of all the mass spectrometry data. Peptide map of recombinant PsbO is shown in **Appendix A, Figure 2.A-2**.

2.2.4 Data analysis

A total of 61 peptides providing 100% coverage were analyzed by Sierra Analytics HDExaminer, (version 2.3, Sierra Analytics, Modesto, CA). The same software was used for hybrid significance testing. In HDExaminer, each peptide with high quality mass spectra in a single charge state was chosen to represent HX-MS data. Spectra were manually checked and verified for all replicates. For each peptide with unimodal spectra, deuterium uptake was calculated by the difference between the centroid mass of the deuterated peptide and the centroid mass of the undeuterated control. Hybrid significance testing[25] was used to find the significant differences at 99% confidence. Unexpectedly, our denatured maximally deuterated experimental data showed slightly lower deuterium uptake for each peptides than the peptides labeled for 72000 s. Because of this, we treated 72000 s as maximal deuteration for each peptides. HX is quantified as a percentage:

$$HX_t = \frac{m_t - m_0}{m_{72000} - m_0} \times 100\%$$

Where, *m* is the peptide mass and the subscripts are the labeling times. Peptides with bimodal spectra were analyzed as explained in the Results section. The structure of PsbO bound to PSII (3JCU) was used to display the of HX-MS data for both released PsbO and recombinant PsbO using PyMol (the PyMOL Molecular Graphics System; Schrodinger LLC, San Diego, CA, USA). Interfacial residues of PsbO bound to PSII were identified using PDBePISA using 3JCU.[26] PsbO residues with buried surface area greater than 0.00 $Å^2$ were considered interfacial residues.

2.3 Results

2.3.1 Recombinant PsbO as a model system

Much of the understanding about bound PsbO structure has been derived from the crystal structure of thermophilic bacteria photosystem II (1.9 Å resolution)[1] and spinach photosystem II (3.2 Å resolution).[1, 27] For higher-order plants and algae, crystal structures are not currently available of an isolated PsbO. Thus, our understanding of PsbO structure is based on studies with recombinant or released PsbO or native PsbO bound to PSII. The structure of unbound PsbO has only been investigated using low resolution techniques like far UV CD, FTIR, and SAXS. Based on these techniques, the secondary structure of a released PsbO was found to be 2%-27% α-helix, 33%-38% β-sheet, 15%-27% turn, and 35%-44% random coil.[29-32] Isolated PsbO has been described as either a natively unfolded polypeptide or molten globular protein, but all the authors found that isolated PsbO contains a high percentage of β-sheet and a high percentage of random coil from their spectroscopic studies. Previous work has established that *E. coli* can express recombinant PsbO and that this recombinant derived PsbO binds to the PSII with the same stoichiometry as native PsbO. Also, after binding to PSII, recombinant PsbO can restore PSII oxygen evolution activity to the same level that native PsbO does. So, recombinant PsbO was

found to be functionally identical to native PsbO after the reconstitution with PSII.[33, 34] In our study, any detectable HX difference between the PsbO extracted from spinach PSII (referred to as "released PsbO") and *E. coli*-derived recombinant PsbO is evidence of a persistent template effect of PSII on released PsbO that is absent from recombinant PsbO that has not bound to PSII.[21]

2.3.2 PsbO exchanges by both EX1 and EX2 mechanisms

We carried out HX labeling on released and recombinant PsbO from 20 s to 72000 s, the proteins were then digested, and peptides were analyzed by mass spectrometry. Representative mass spectra of recombinant PsbO are shown in **Figure 2.1**. Analyzed data of our peptide level HX-MS experiment showed mass spectra with unimodal isotopic signature (indicating an EX2 exchange mechanism) and bimodal isotopic signature (indicating an EX1 exchange mechanism[35]).

Figure 2.1a shows representative spectra for peptides 18-38 and 115-126 with unimodal isotopic distribution (EX2 mechanism). In the figure, the left vertical lines indicate average m/z of the undeuterated population and the right vertical lines indicate average m/z of the maximally deuterated populations. As the deuteration time increases, the unimodal isotopic distributions go progressively from lower m/z value to higher m/z value, although the rate of deuteration depends on the type of protein structure. For the 18-38 segment for recombinant PsbO, at 20 s deuterium was already mostly exchanged and at 1000 s deuterium exchange was complete. For the 115-126 segments, deuterium exchange slowly progressed from 20 s to 72000 s with a unimodal distribution and maximum deuterium exchange was reached at 10000 s. These unimodal isotopic signatures indicates that the HX of these regions of PsbO followed an EX2 mechanism.

Figure 2.1b shows the mass spectra from recombinant PsbO of representative peptides 38-56, 127-144, and 218-241 with bimodal isotopic distributions. Region 38-56 shows two isotopic distributions with different abundances at 20 s. At that labelling time, higher abundance is the

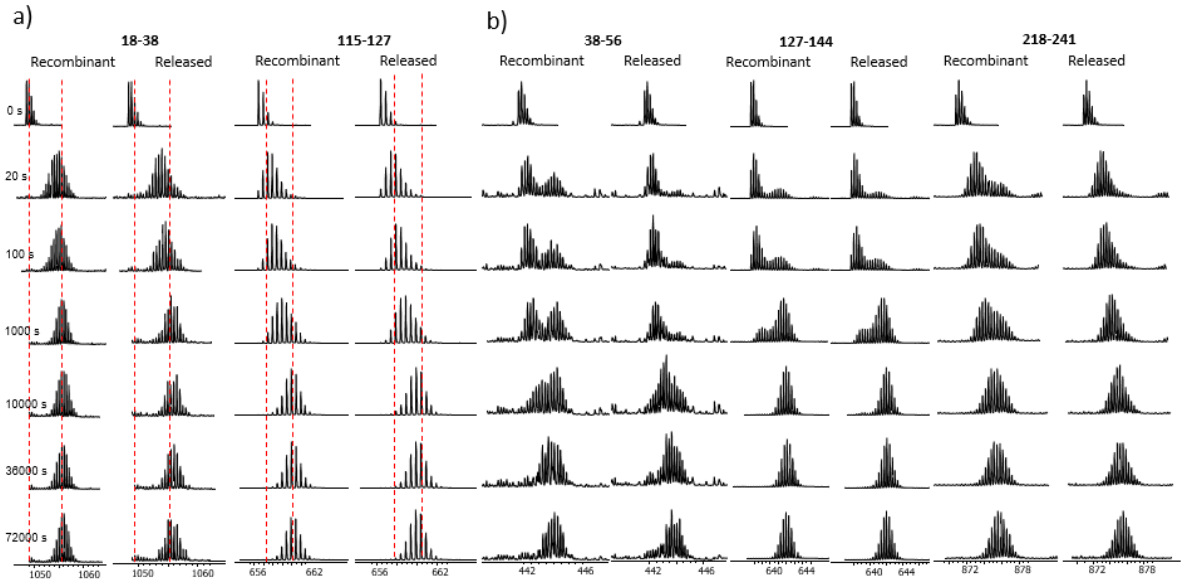

Figure 2.1. (a) Mass spectra of unimodal isotopic signature (b) mass spectra of bimodal isotopic signature.

undeuterated population and lower abundance is the deuterated population. At 1000 s, deuterated and undeuterated population abundance are close to equal. Complete deuteration was observed at 36000 s. The same pattern of bimodal distribution is also observed in segment 218-241. Region 127-144 also showed two isotopic distribution with two different abundances at 20 s the undeuterated population was higher in abundance. As labelling time increases, the deuterated populations increased and the undeuterated populations decreased. The equal abundance of deuterated and undeuterated population is between 100 s to 1000 s. At 10000 s, complete deuteration was observed for this region. Bimodal isotopic distributions were also seen in regions 86-109 and 202-217. All spectra from regions with bimodal distributions are included in the **Appendix A, Figure 2.A-3**.

In HX-MS, the EX1 isotopic signature is an uncommon observation. Mass spectra with bimodal distributions can arise from experimental artifacts. These spectra are sometimes misassigned as evidence of EX1 exchange. Bimodal isotopic distribution can appear because of protein aggregation, abnormal back exchange or chromatographic carryover.[36, 37] When bimodal distribution is seen as a result of protein aggregation, typically the undeuterated population of that bimodal distribution should be constant for all labeling time points, because, the aggregated sites restrict protein motion and thus prevent deuterium exchange. In our cases, we do not see the undeuterated population after 36000 s for any of our mass spectra in (see **Figure 2.1b** and **Appendix A Figure 2.A-3, residues 86-109**). Diminishing of bimodal signature after 36000 s indicates that our bimodal spectra are not due to protein aggregation. When bimodal distribution appears due to abnormal back exchange, all peptides should show mass spectra with bimodal signatures. As **Figure 2.1** shows, we can distinctly see mass spectra of peptides with bimodal signature and mass spectra of peptides with unimodal signature. Thus, abnormal back-exchange is not the cause of the bimodal spectra. Bimodal distributions also can be seen due to chromatographic carryover of peptides. To rule out peptide carryover, we conducted carryover study with recombinant PsbO with the same method of the peptide level HX-MS experiment followed by running a blank. Comparing the total ion chromatogram (TIC) of recombinant PsbO with blank TIC, shows that no peptides were significantly carried over in the blank run (**Appendix A, Figure 2.A-4**). Another separate experiment, denatured deuteration control, was carried out to see whether bimodal spectra were caused by carryover and also to measure maximum deuterium uptake by each peptide. In the denatured deuteration control experiment, d_4-urea was used to label the protein and also fully denature the PsbO. Deuterium labeling of a protein under denaturing conditions will cause PsbO to lose its native structure and refolding ability and thus PsbO would

show unimodal isotopic distributions with maximum deuteration. Thus, under denaturing condition, bimodal isotopic distribution would be evidence of carryover artifact. Our denatured deuteration control experiment showed unimodal isotopic distribution for all peptides (**Appendix A, Figure 2.A-6**). Therefore, we conclude that bimodal signatures were due to a native phenomenon during labeling, not a carryover problem. Thus, based on our critical assessment of control experiments, the bimodal isotopic signatures of recombinant PsbO were not an artifact, they are evidence of EX1 exchange, indicating that some regions of PsbO undergo slow, correlated unfolding.

2.3.3 Recombinant PsbO has a core folded structure

EX2 exchange was quantified in terms of mass increase by measuring the average centroid mass at each labelling time compared to the centroid mass of non-deuterated control. **Figure 2.2** shows representative uptake plots for regions of PsbO that exchange by EX2. To aid in the analysis, we consider the HX effects in the context of the structure of PsbO in complex with PSII. Uptake plots for recombinant PsbO can be divided into three categories: slow HX ($HX_{20\,s} \leq 50\%$, fig. 2a), intermediate HX ($50\% < HX_{20\,s} < 90\%$, fig.2b) and fast HX ($HX_{20\,s} > 90\%$, fig. 2c). Slow HX by recombinant PsbO was found in residues 111-26 (sheet c, loop g, sheet d) and 242-247 (sheet j, loop p). Fast HX by recombinant PsbO was found in residues 1-17 (loop a, helix A, loop b, helix B), 58-77 (sheet a, loop e), and 155-170 (loop j). Intermediate HX was found in residues 18-38 (helix B, loop c, helix C, loop d), 78-86 (loop e), and 171-201 (loop j, helix E, loop k, helix F, loop l, sheet g) (**Appendix A, table A-1**).

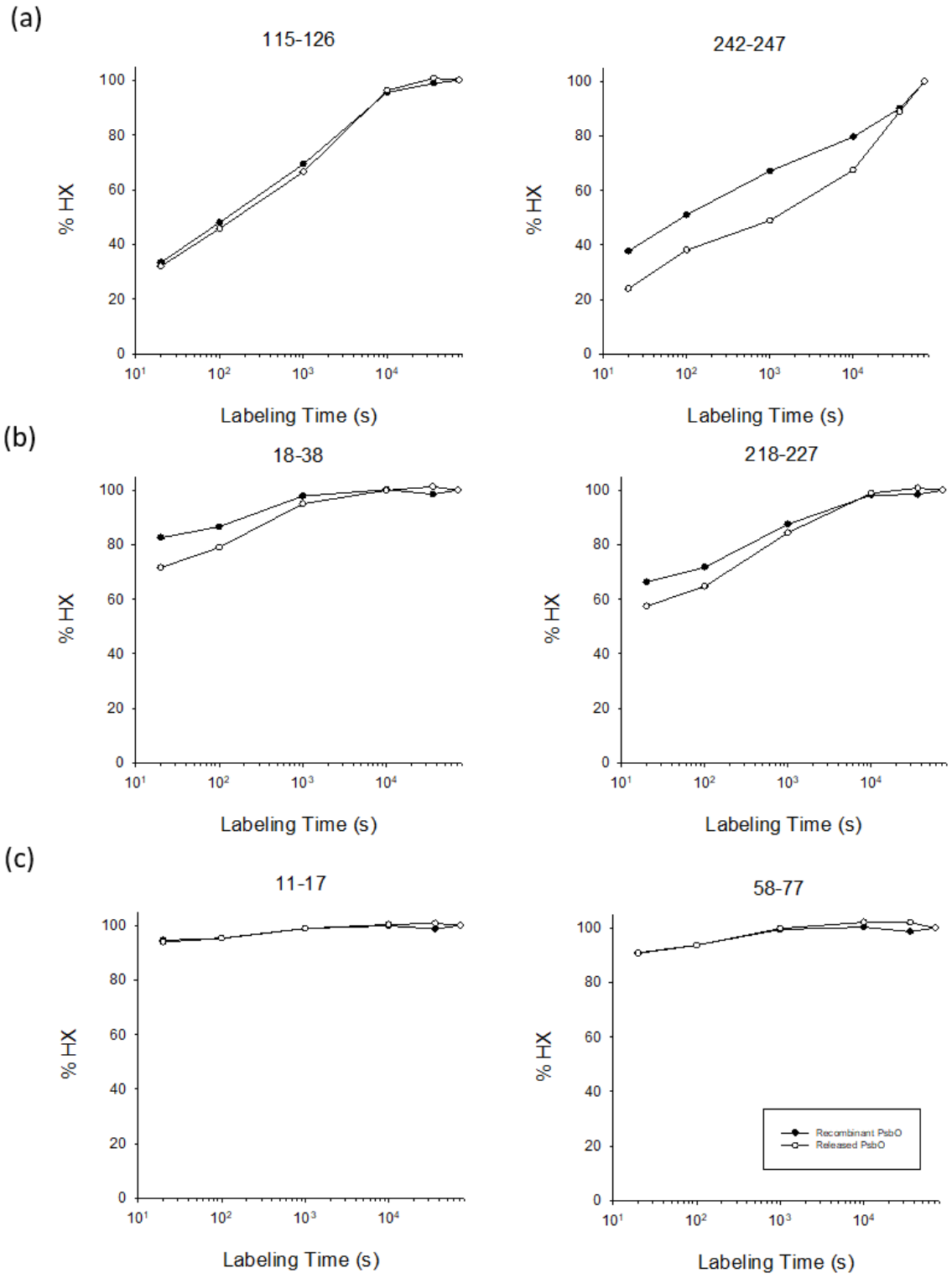

Figure 2.2. Deuterium uptake plots of unimodal isotopic profile (a) slow HX (slow HX (HX20 s ≤ 50%) (b) intermediate HX (50% < $HX_{20\,s}$ < 90%), and (c) fast HX region ($HX_{20\,s}$ > 90%).

Figure 2.3a shows that EX1 exchange by recombinant PsbO (in magenta) is only in the region of PsbO that forms a β barrel in the PSII complex. Regions exchanging by the EX1 mechanism include residues 38-56 (loop d, sheet a), 202-217 (sheet g, loop m, sheet h), and 218-241 (sheet h, loop n, sheet i, loop o, sheet j) which are all on the face of the β barrel (sheet a, g, h, i, j) that is solvent exposed when PsbO is in complex with PSII (referred to here as the "front side" of the β barrel). Exchange by EX1 mechanism also occurs in residues 86-109 (loop e, sheet b, loop f) and 127-144 (sheet d, loop h, sheet e, loop i, helix D, sheet f) which are on the back side of the β barrel (sheet b, d, e, f). EX1 means there is slow, local unfolding in these regions.

There are different timescales for the local unfolding. To follow the local unfolding timescales, we consider the half time ($t_{½}$) for each region that undergoes EX1 exchange. Half-time ($t_{½}$) is the HX labeling time when the abundance of undeuterated and deuterated isotopic distributions are equal. EX1 exchange by recombinant PsbO at residues 38-56, 86-109, and 218-241 takes approximately 10^3 s to reach the $t_{½}$. In the residues 202-217, the $t_{½}$ is approximately 36000 s. In the residues 127-144, the $t_{½}$ for HX is between 100 s and 1000 s. 127-144 unfolds more readily than other EX1 exchange regions and 202-217 is held relatively tightly. We have categorized the EX1 exchange into three categories: slow EX1 ($t_{1/2} > 36000$ s), intermediate EX1 (10^3 s $< t_{1/2} < 36000$ s) and fast EX1 ($t_{1/2} \leq 10^3$ s). **Figure 2.3b** shows the slow HX regions (in blue), intermediate HX regions (in green), and fast HX regions (in yellow) of all the EX2 and EX1 exchange data combined. Slow HX regions are in the β barrel as revealed by our EX1 data (residues 38-56, 86-109, 127-144, 202-217, and 218-241) and EX2 data (residues 111-127, 242-247). Fast HX regions are in coils, α-helix and very small part in β-sheet as revealed by our EX2 exchange data. According to slow HX data, roughly half of the PsbO residues are located in structured

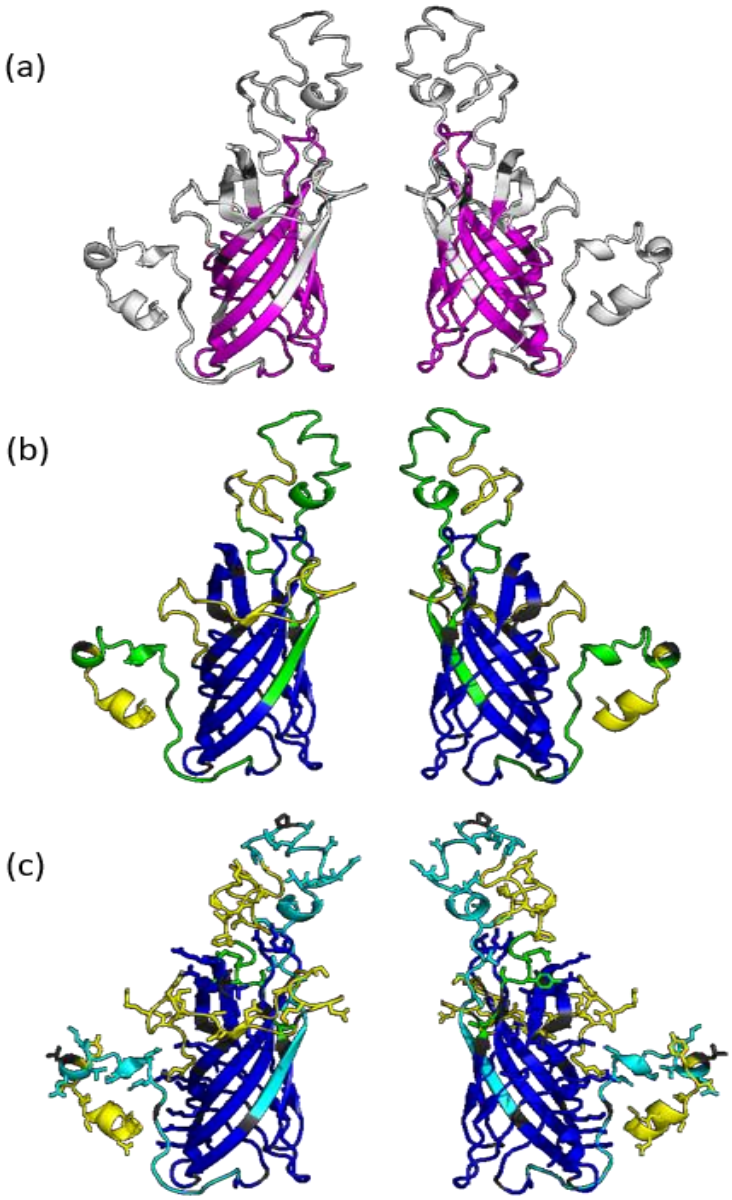

Figure 2.3. (a) Regions exhibiting bimodal HX (magenta), no coverage (dark grey) (b) regions exhibiting bimodal or slow HX in recombinant PsbO (blue), regions of fast HX (yellow), intermediate HX (green) no coverage (dark grey), (c) effects of PSII templating after PsbO is released, cyan: intermediate HX regions in recombinant PsbO where HX was slower in released PsbO. Sticks: PSII interfacial residues, blue: slow HX by released PsbO, yellow: fast HX released PsbO, green: intermediate by released PsbO

regions of recombinant PsbO. Overall our HX results indicate that recombinant PsbO is a molten globular protein because it has core structured β barrel region with random coils and α-helix.

2.3.4 PSII exerts a persistent effect on PsbO following PsbO release

As a previous IR study showed that there were structural differences between released PsbO and recombinant PsbO,[21] so our major focus of this study was to investigate the template effect on released PsbO at higher resolution. To understand the effects of PSII on PsbO following release from PSII, we compared HX by PsbO from spinach PSII, released by $CaCl_2$ treatment, with HX by recombinant PsbO. [19, 38, 39]

Overall, the effect of templating by PSII is to slow HX throughout the PsbO chain, though the magnitude of the effects were not uniform. Even though recombinant PsbO has a structured core, our HX-MS measurements showed HX slowing in released PsbO in regions that exchange by EX2 and EX1 HX. We identified the templating effect of PSII on released PsbO for those regions that exchanged by EX2 kinetics using hybrid statistical significance testing[25] at 99% confidence (**Appendix A, Figure 2.A-5**). We detected slower HX in residues 18-38 (helix B, loop c, helix C, loop d), 111-126 (sheet c, loop g, sheet d), 183-201 (loop k, helix F, loop l, sheet g), 171-201 (Loop j, helix E, loop k, helix F, loop l, sheet g) and 242-247 (sheet j, loop p).

For EX1, we compared $t_{½}$ values from recombinant PsbO with $t_{½}$ values from released PsbO. HX was slowed in residues 38-56 (loop d, sheet a), 202-217 (sheet g, loop m, sheet h), and 218-241 (sheet h, loop n, sheet i, loop o, sheet j), which reside in the beta barrel (**Figure 2.3c**). In the released PsbO residues 38-56, we see bimodal distribution appeared at 20 s like recombinant PsbO (**Figure 2.1b**). But the important difference is the pattern of bimodal signature between released PsbO and recombinant PsbO. Templating by PSII caused HX to slow down in residues

38-56 and 218-241, $t_{½}$ for released PsbO is between 10^3 s and 10^4 s (in intermediate EX1), while recombinant PsbO is approximately at 10^3 s (fast EX1). At residues 202-217, $t_{½}$ for released PsbO is greater than our longest labeling time (72000 s) (slow EX1), while $t_{½}$ for recombinant PsbO is approximately at 36000 s (intermediate EX1). For EX1 exchange region, released PsbO showed overall slower HX with substantial slowing at residues 202-217. Two regions of released PsbO, 86-109 (loop e, sheet b, loop f) and 127-144 (sheet d, loop h, sheet e, loop i, helix D, sheet f), had fast EX1 exchange identical to recombinant PsbO. Thus, these two regions are structurally identical for both recombinant and released PsbO.

Figure 2.3c shows the mapping of the PSII templating effect on PsbO. The structured core of recombinant PsbO (as also shown in Figure 3b) that exchanged slowly is shown in blue, regions outside of the structured core where HX was slowed by templating are shown in cyan and regions that were not significantly affected by PSII are shown in yellow. Our HX data showed evidence of PSII templating on released PsbO: in regions that exchange by EX2, we found substantial HX slowing in residues 18-38 (helix B, loop c, helix C, loop d), 218-227 (sheet h, loop n, sheet i, loop o), and 242-247 (sheet j, loop p). Evidence of the templating effect by PSII is also in regions that exchange by EX1 region at residues 38-56 (loop d, sheet a) and 218-241 (sheet h, loop n, sheet i, loop o, sheet j). There was also a more substantial HX slowing at residues 202-217 (sheet g, loop m, sheet h).

Figure 2.3c shows the overall template effects of PSII on released PsbO. Because HX was slowed in all regions by PSII templating, the cyan regions in **Figure 2.3c** identify regions of intermediate HX in recombinant PsbO that became significantly slowed by PSII templating. These slowed regions are in 18-38 (helix B, loop c, helix C, loop d), 111-126 (sheet c, loop g, sheet d),

183-201 (loop k, helix F, loop l, sheet g), 171-201 (Loop j, helix E, loop k, helix F, loop l, sheet g) and 242-247 (sheet j, loop p).

After mapping the PSII template effect onto PsbO, we tried to identify correlations between regions exhibiting a strong template effect and regions that formed the interface between PsbO and PSII. **Figure 2.3c** also shows PSII interfacial residues in stick representation. EX2 regions with slowed HX are in cyan color (residues 18-38 and 171-201). Many of these residues were interfacial residues (residues 18-21, 23-27, 29, 171-176, and 178-183) before PsbO was released from PSII. EX2 regions with slowed HX are in blue color (residues 111-126, 218-227, and 242-247). Many of these residues are also interfacial residues (residues 111-112, 114, 116-120, 124, 126, 226, and 244). These data suggest that in EX2 regions, regions with slowed HX were interfacial residues and that PsbO retains the template effect after being released from PSII. However, fast HX regions, in yellow color (residues 9-17, 58-86 and 155-170) with interfacial residues 9, 12-17, 64-67,73-80, 82, 155-161, 165, 167 and 170, and intermediate HX (residues 145-155) with interfacial residues on 146, 148-152, 154-155 have no statistically significant HX slowing even though both fast and intermediate HX slowing regions have interfacial residues with PSII. In the EX1 regions, show in blue, (residues 38-56, 202-217 and 218-241) have interfacial residues on 48, 51, 212, 226, and 229-230. Our HX found the strongest template effect in that all of these bimodal regions in released PsbO with substantial template effect in 202-217. However, EX1 region in blue color (residues 86-109 and 127-144) have interfacial residues on 86-87, 89, 105-109, and 130 showed no HX difference. Overall, in bimodal region, limited interfacial contact is observed. The important conclusion here is that all newly-stabilized regions are interfacial, but that not all interfacial regions become stabilized by PSII templating.

2.4 Discussion

A previous study found that bacterially derived recombinant PsbO restores the oxygen evolution activity upon binding to PSII, demonstrating that recombinant PsbO is functionally identical to released PsbO even though the protein source is different.[40] The structure of PSII complexed with native or recombinant PsbO might be identical since both of them can restore PSII activities like oxygen evolution. Based on IR spectroscopy, bacterially expressed recombinant PsbO was not an unfolded protein, but the structures of recombinant PsbO complexed with PSII and recombinant PsbO in solution were dramatically different.[21] So PSII templates the PsbO when PsbO binds to PSII and PsbO retains template effect upon release from PSII. The previous IR study found that the released PsbO in solution has higher content of secondary structure such as β-sheet, turns, and helices. Comparing solution structure of released PsbO and naïve recombinant PsbO by IR revealed structural differences. This structural difference was attributed as template effect. Now the new question is which specific regions of PsbO actually retain the template effect and how it compares with untemplated PsbO.

To elucidate the template effect of PSII on PsbO at peptide resolution, one option would be to compare recombinant PsbO before binding and after release from PSII. The challenge with this option is to get pure PsbO. As shown in our intact protein mass data (**Appendix A, Figure 2A-7**), recombinant PsbO sample released from spinach PSII was contaminated with spinach PsbO. The issue with the released sample is that a single spectrum of a peptide can come from two sources: spinach and recombinant, so PsbO peptide spectra would be a mixture of spinach PsbO and recombinant PsbO. So to investigate the template effect of PSII on PsbO at peptide resolution, we compared the PsbO released from spinach PSII with naive recombinant PsbO like

the previous IR study did.[21] In our study, we explored the template effect of PSII on PsbO using a higher resolution technique, HX-MS.

In our study, we found recombinant PsbO is not an unfolded protein, rather, this protein has roughly half of its residues located in structured regions (slow HX), mainly in the region that forms a β-barrel in the PSII complex. Our HX data show that recombinant PsbO undergoes reversible local unfolding on the 10-1000 s timescale for residue location at loops d-f, h-i, n, and o; sheets a-b, d-f, and h-j; and helix D and 36000 s timescale for sheets g-h, and loop m segment indicating that PsbO has at least a loosely structured β-barrel with hydrogen bonding that is weaker than the released PsbO (**Figure 2.3a**). Residues located in sheet c and d (111-126), and sheet j, loop p (242-247) are also a part of the β-barrel that undergo slow HX. Overall recombinant PsbO has core β-barrel that undergoes slow HX and the rest of the part are intermediate to fast HX (major parts are in loops).

Binding/release from PSII imprints additional stability onto PsbO in the regions of slow HX (EX2), intermediate HX (EX2), and slow EX1 HX (in sheet a, g, h, i, j, front side of β-barrel). The slow HX on the front side of the β-barrel region of released PsbO is due to a more tightly held hydrogen bond network. This tightly held hydrogen bond is the stabilization effect from PSII that is retained by released PsbO. Some PsbO interfacial regions that exchanged by EX2 kinetics in released PsbO did not show any HX differences. There are several reasons that could cause this. One reason could be because the extraction process has an effect on PsbO released from the PSII complex. Another reason could be that there are template effects in these regions, but that our experimental design did not allow us to detect the effect. In our HX, the earliest labeling time was 20 s. It may be that 20 s of HX was too long to detect HX differences in regions that exchange quickly. Since those residues are located in the loop region where hydrogen bonds are weaker they

exchange rapidly as shown by the high percentage of exchange at 20 s labeling time, so millisecond labeling might be required to detect HX differences in the loop regions.

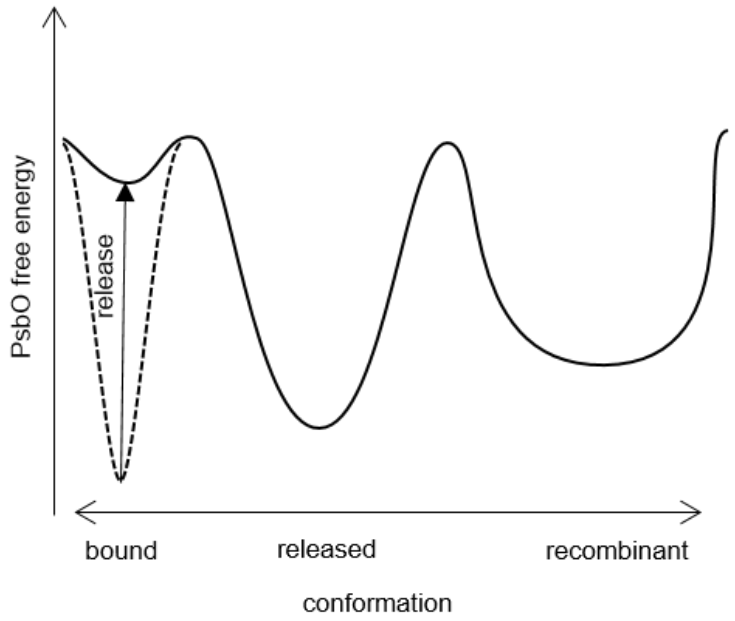

Figure 2.4. Thermodynamic model of templating of PsbO

Figure 4 shows a thermodynamic representation of our overall HX findings about PsbO structure. In this model, three important regions are shown: PsbO in the PSII bound conformation, released PsbO, and recombinant PsbO. While bound PsbO is represented by a deep energy minimum, released and recombinant PsbO energetic minima represent broad conformational ensembles. PsbO bound to PSII is the most stable state of PsbO. Upon release from PSII, the bound conformation of PsbO becomes highly unstable because of the loss of many intermolecular contacts to PSII causing the major population of PsbO to attain a partially unfolded conformation. Recombinantly expressed PsbO represents a different conformational ensemble that is less stable than released PsbO and separated from the released conformational ensemble by a high barrier. The template effect in its structure is retained because of high energetic barrier between the

released and recombinant states. PsbO reorganizes its structure when it binds to PSII, and when it releases from PSII, it retain templates effect from PSII and that has been shown in our HX study.

PSII is prone to damage by overwhelming light and heat.[41] Intrinsic subunit D1 experiences the most damage out of all subunits in PSII. During repair, PSII is partially dissembled, where damaged D1 is replaced by a new D1 subunit, and the old D1 is degraded by proteases.[42-45] During the repair process, it has been found that another intrinsic subunit, CP43, and extrinsic subunit PsbO are also released from PSII. Unbound soluble PsbO has been detected in thylakoid lumen.[46, 47] Free PsbO may be involved in maintaining PSII hemostasis, by acting as chaperone for other released subunits.[41] In vitro, PsbO plays a key role in preventing aggregation of D1 and CP43, and regulating D1 interaction with CP43. How PsbO regulates the interaction of D1 and CP43 is unknown. It was suggested that the extended conformation of released PsbO might control the interaction of D1 and CP43. Thus it is essential to know what part of released PsbO is extended to understand how released PsbO controls the interaction of D1 and CP43. Since our HX study suggests PsbO has β-barrel core (~50% residues) therefore the other 50 % residues are flexible and intermediate. Thus, the intermediate and flexible regions might be acting as extended part of free PsbO for the regulation of D1 and CP43 interaction. In future, conformational study of PSII-PsbO complex should be studied with higher resolution techniques to elucidate the role of PsbO in photodamage repair and along that way, more interesting structural study might give valuable insight for other contributions from PsbO.

2.5 Appendix A

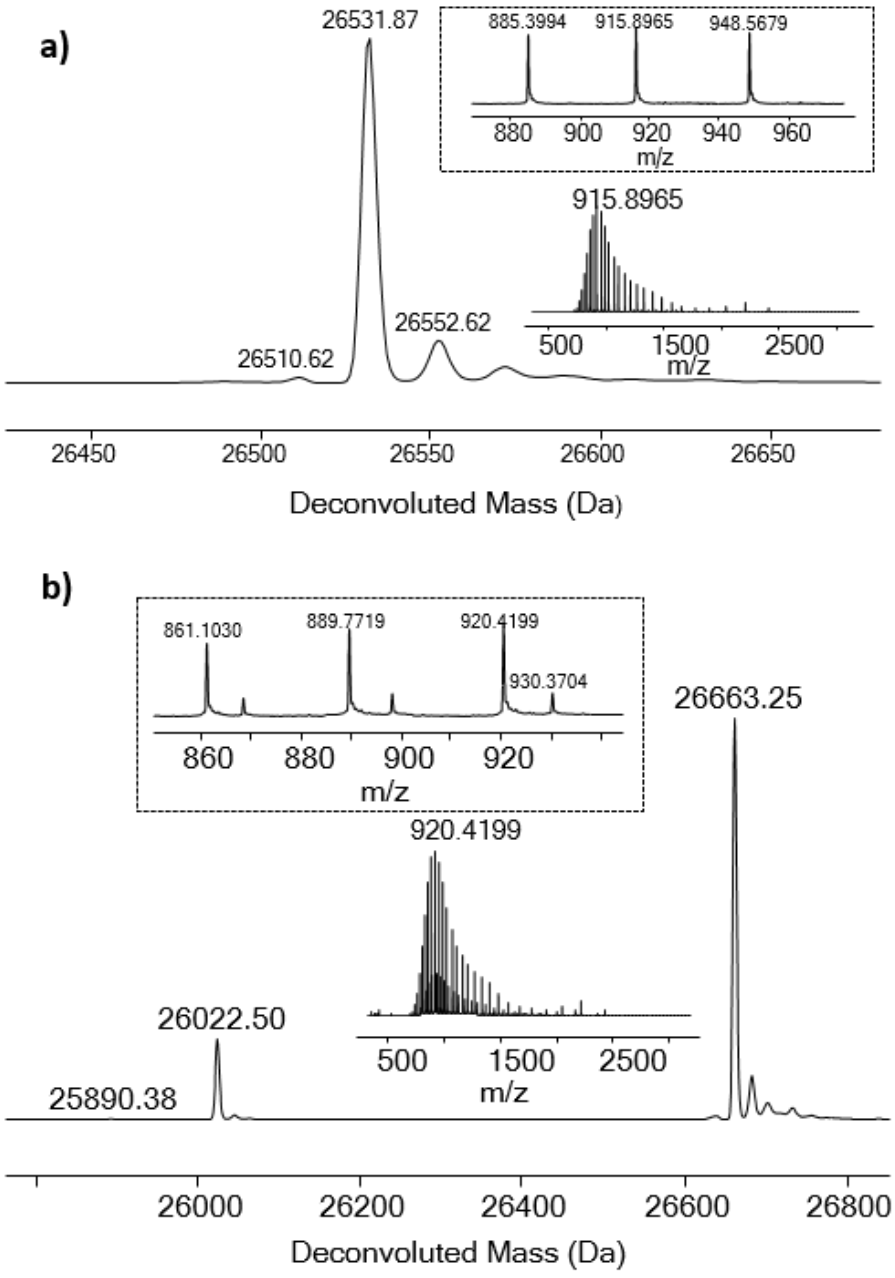

Figure 2.A-1. Deconvoluted spectrum with inlaid full and zoomed raw mass spectrum (a) released PsbO (b) recombinant PsbO

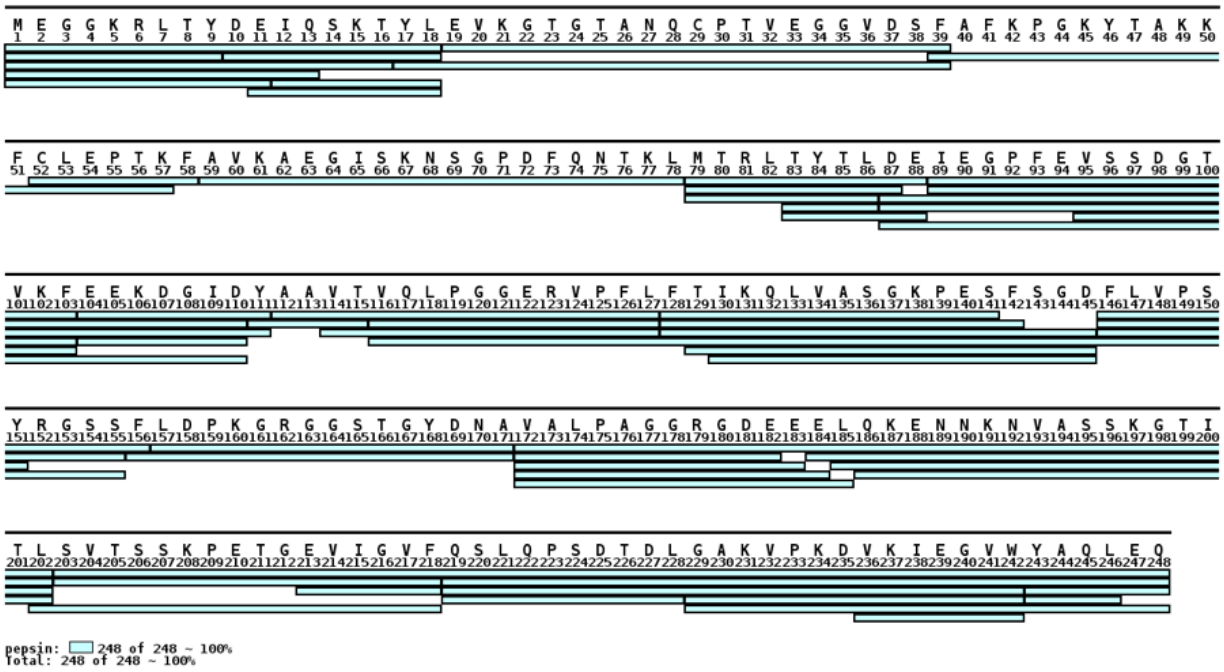

Figure 2.A-2. Peptic peptide mapping of PsbO (Kavan, D. and Man, P. MSTools - Web based application for visualization and presentation of HXMS data" Int. J. Mass Spectrom. 2011, 302: 53-58)

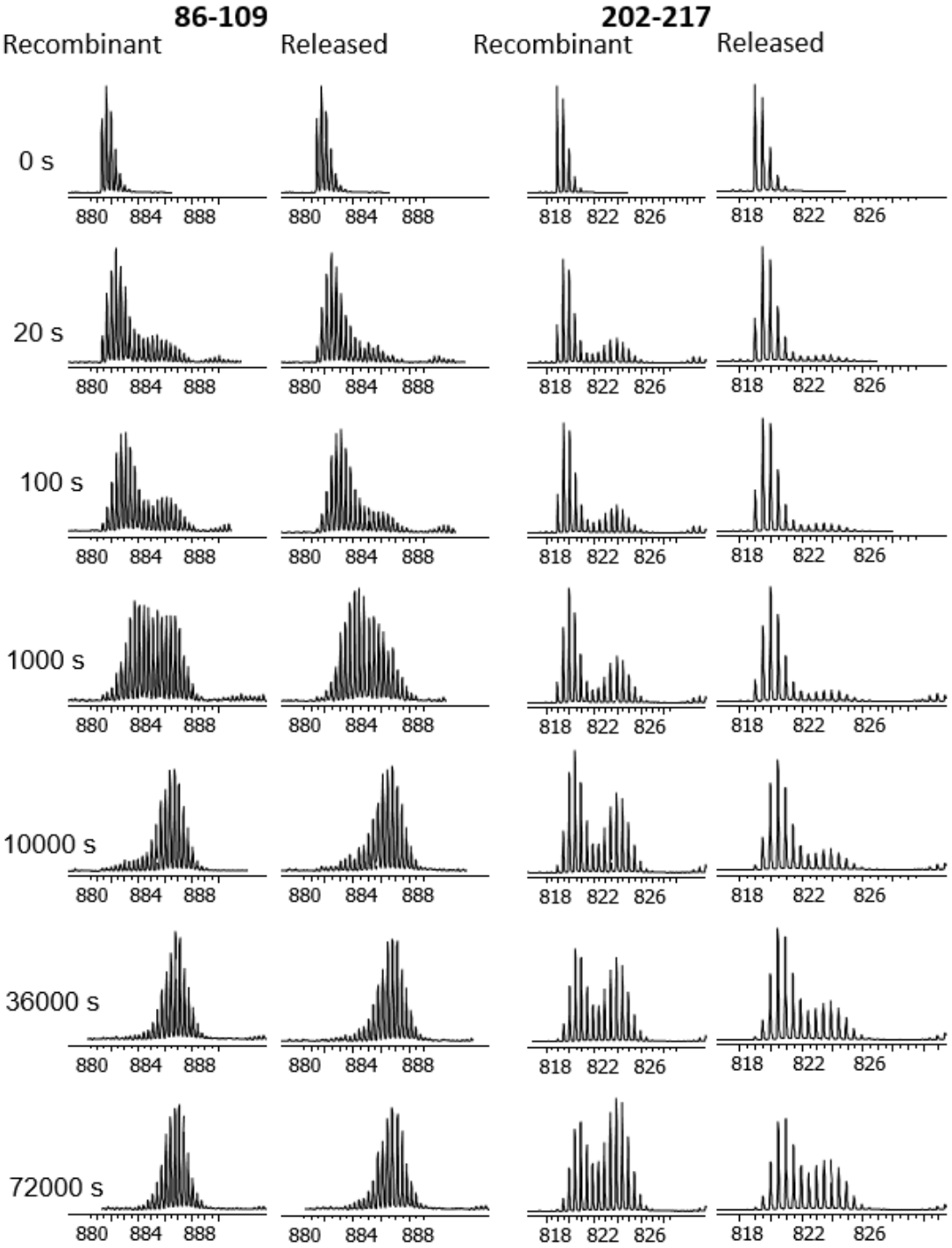

Figure 2.A-3. Mass spectra showing bimodal isotopic signature, residues 86-109 and 202-217.

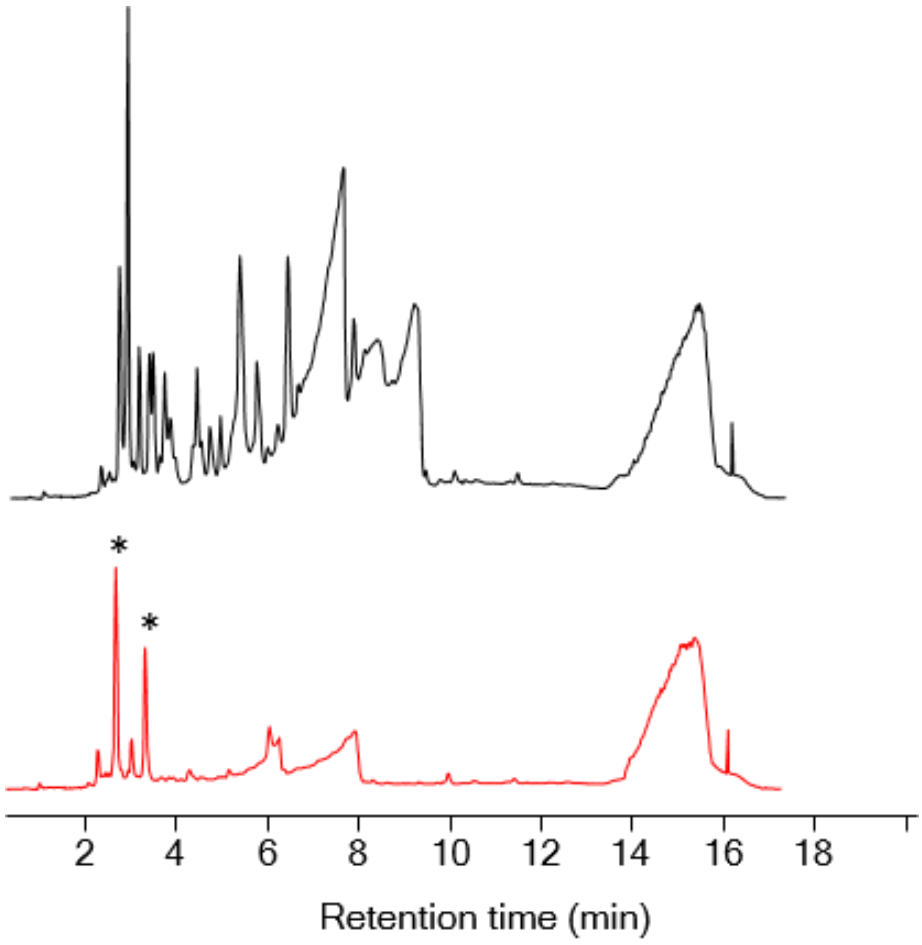

Figure 2.A-4. Total ion chromatograms of peptic digest of PsbO (black) and a subsequent digestion blank (red). HX-MS data were acquired between 2-12 min. Although the blank chromatogram shows a few abundant carryover peaks, marked with asterisks, these peaks are not part of our analysis

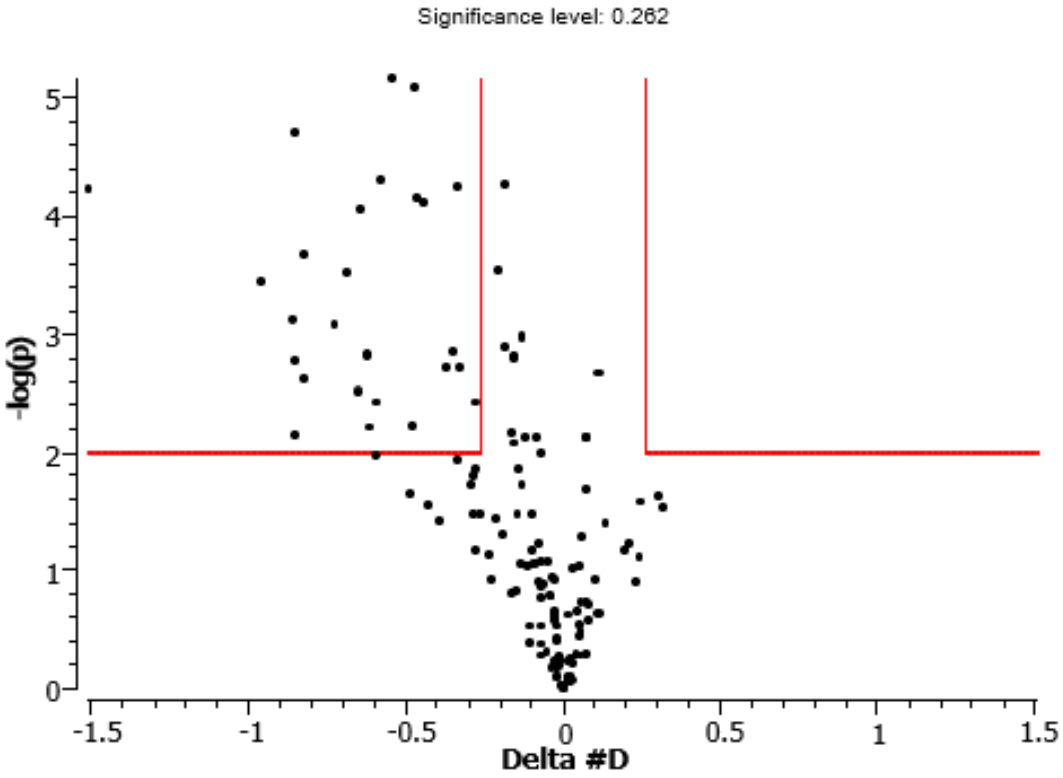

Figure 2.A-5. Hybrid significance testing of HX differences between released and recombinant PsbO represented by a volcano plot. The significance criteria are $p < 0.01$ and $|\Delta D| > 0.262$ Da (red solid lines).

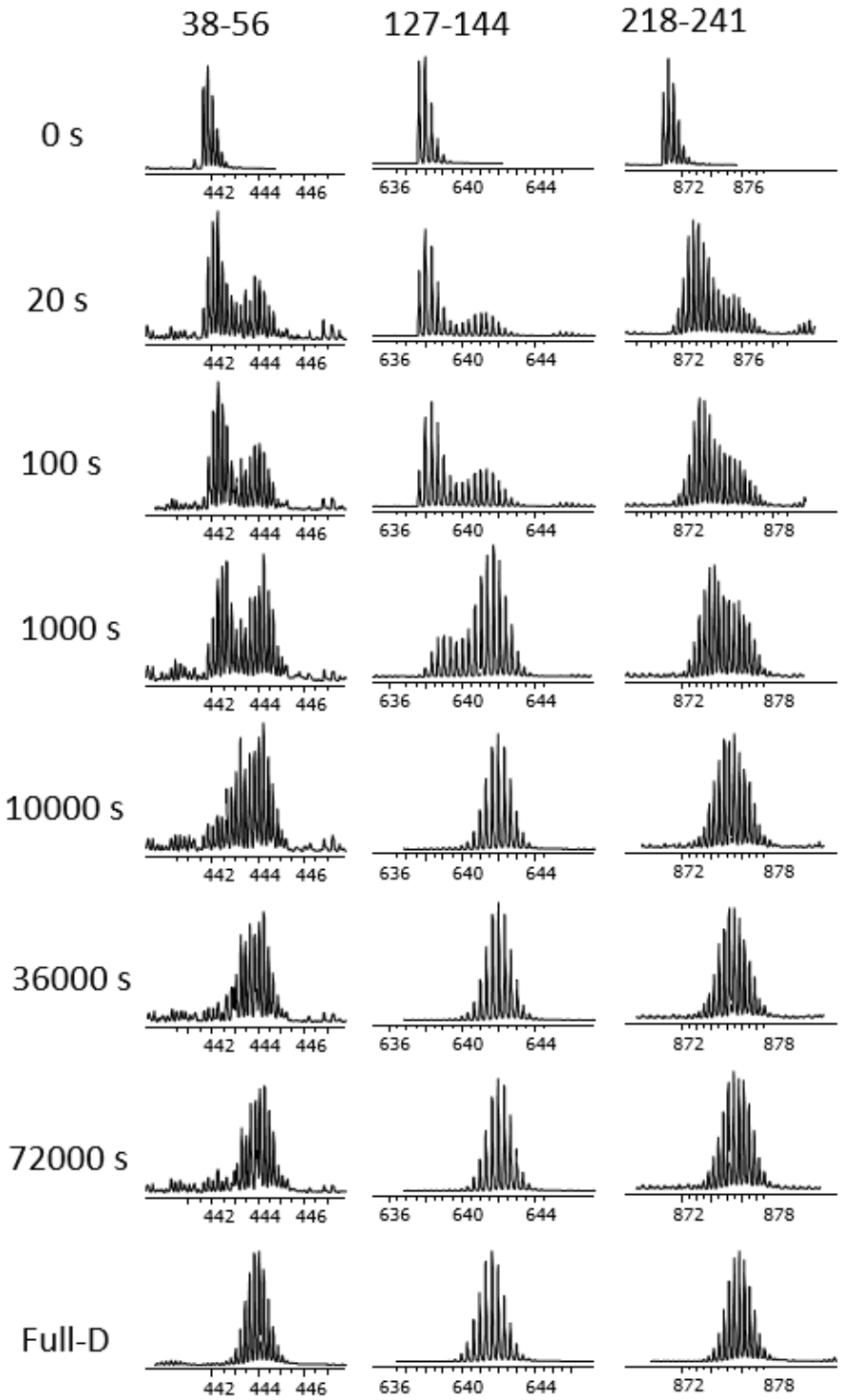

Figure 2.A-6. Mass spectra of bimodal isotopic signatures of residues 38-56, 127-144 and 218-241 disappeared in full-D labeling condition

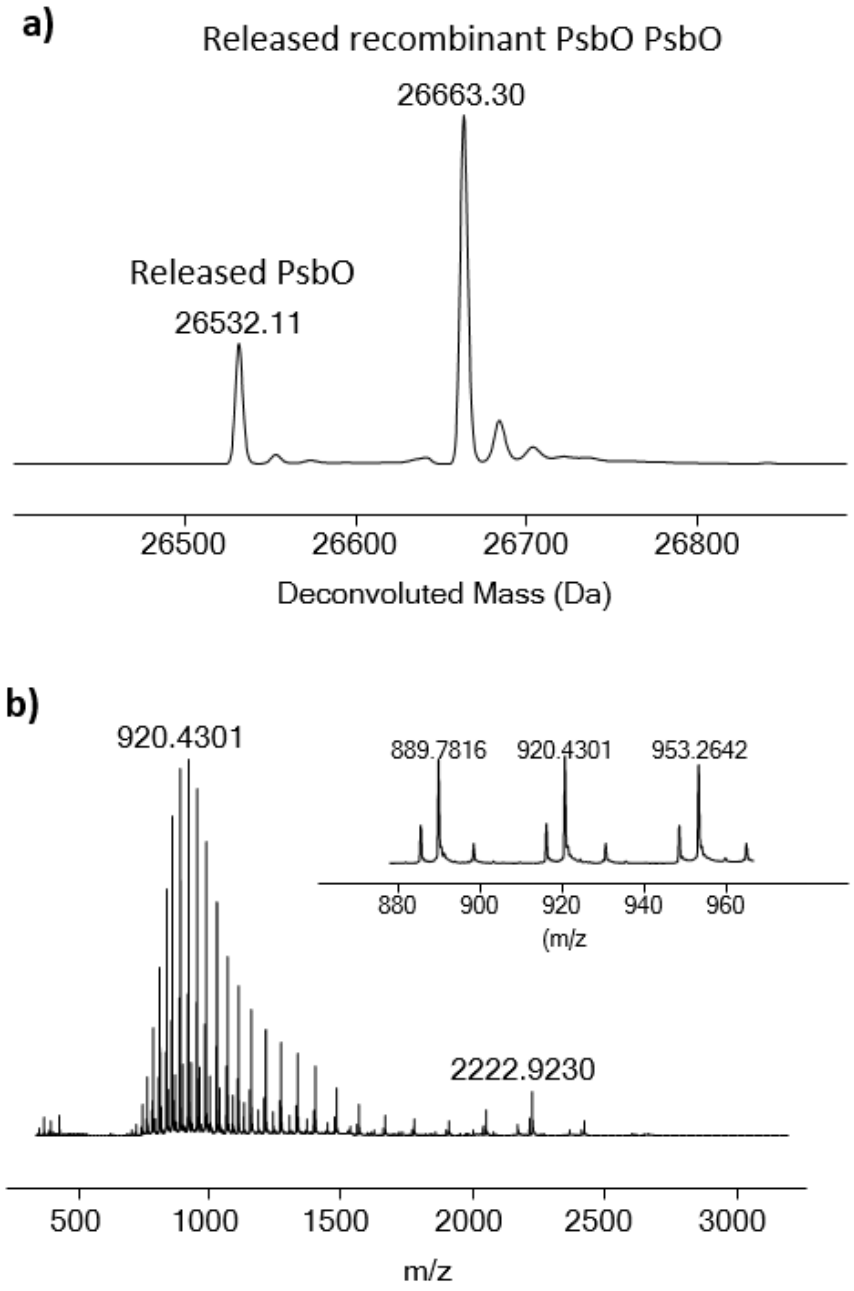

Figure 2.A-7. Recombinant PsbO released from PSII is contaminated with spinach PsbO (a) deconvoluted mass (b) raw mass spectrum inlaid zoomed m/z profile

Table A-1. HX defined categories of PsbO

Residue number	Secondary structural elements	Recombinant PsbO HX category	Released PsbO HX category
1-8	Loop a, helix A	Fast EX2	NA
9-17	Helix A, loop b, helix B	Fast EX2	Fast EX2
18-38	Helix B, loop c, helix C, loop d	Intermediate EX2	Intermediate EX2
38-56	Loop d, sheet a	Fast EX1	Intermediate EX1
58-77	sheet a, loop e	Fast EX2	Fast EX2
78-86	loop e	Intermediate EX2	Intermediate EX2
86-109	Loop e, sheet b, loop f	Fast EX1	Fast EX1
103-109	Loop f	Intermediate EX2	Intermediate EX2
111-126	Sheet c, loop g, sheet d	Slow EX2	Slow EX2
127-144	Sheet d, loop h, sheet e, loop i, helix D, sheet f	Fast EX1	Fast EX1
145-155	Sheet f, loop j	Intermediate EX2	Intermediate EX2
155-170	Loop j	fast EX2	fast EX2
171-201	Loop j, helix E, loop k, helix F, loop l, sheet g	Intermediate EX2	Intermediate EX2
183-201	loop k, helix F, loop l, sheet g	Intermediate EX2	Intermediate EX2
202-217	Sheet g, loop m, sheet h	Intermediate EX1	Slow EX1
218-227	Sheet h, loop n, sheet i, loop o	Intermediate EX2	Intermediate EX2
218-241	Sheet h, loop n, sheet i, loop o, sheet j	Fast EX1	Intermediate EX1
242-247	Sheet j, loop p	Slow EX2	Slow EX2

2.6 References

1. Wei, X.; Su, X.; Cao, P.; Liu, X.; Chang, W.; Li, M.; Zhang, X.; Liu, Z., Structure of spinach photosystem II-LHCII supercomplex at 3.2 A resolution. *Nature* **2016,** *534* (7605), 69-74.

2. Popelkova, H.; Yocum, C. F., PsbO, the manganese-stabilizing protein: analysis of the structure-function relations that provide insights into its role in photosystem II. *J Photochem Photobiol B* **2011,** *104* (1-2), 179-90.

3. Bricker, T. M., Oxygen evolution in the absence of the 33-kilodalton manganese-stabilizing protein. *Biochemistry* **1992,** *31* (19), 4623-4628.

4. Hutchison, R. S.; Steenhuis, J. J.; Yocum, C. F.; Razeghifard, M. R.; Barry, B. A., Deprotonation of the 33-kDa, Extrinsic, Manganese-stabilizing Subunit Accompanies Photooxidation of Manganese in Photosystem II. *Journal of Biological Chemistry* **1999,** *274* (45), 31987-31995.

5. Barry, B. A.; Brahmachari, U.; Obi, C. E.; He, J. N., The intrinsically disordered PsbO subunit of Photosystem II: structure and role in photosynthetic water oxidation. *The FASEB Journal* **2018,** *32* (1_supplement), 795.8-795.8.

6. Gururani, M. A.; Upadhyaya, C. P.; Strasser, R. J.; Yu, J. W.; Park, S. W., Evaluation of abiotic stress tolerance in transgenic potato plants with reduced expression of PSII manganese stabilizing protein. *Plant science* **2013,** *198*, 7-16.

7. Sasi, S.; Venkatesh, J.; Daneshi, R. F.; Gururani, M. A., Photosystem II Extrinsic Proteins and Their Putative Role in Abiotic Stress Tolerance in Higher Plants. *Plants (Basel)* **2018,** *7* (4).

8. Nickelsen, J.; Rengstl, B., Photosystem II assembly: from cyanobacteria to plants. *Annual review of plant biology* **2013,** *64*, 609-635.

9. Pawłowicz, I.; Kosmala, A.; Rapacz, M., Expression pattern of the psbO gene and its involvement in acclimation of the photosynthetic apparatus during abiotic stresses in Festuca arundinacea and F. pratensis. *Acta Physiologiae Plantarum* **2012,** *34* (5), 1915-1924.

10. Yamamoto, Y.; Aminaka, R.; Yoshioka, M.; Khatoon, M.; Komayama, K.; Takenaka, D.; Yamashita, A.; Nijo, N.; Inagawa, K.; Morita, N.; Sasaki, T.; Yamamoto, Y., Quality control of photosystem II: impact of light and heat stresses. *Photosynthesis Research* **2008,** *98* (1), 589-608.

11. Lydakis-Simantiris, N.; Hutchison, R. S.; Betts, S. D.; Barry, B. A.; Yocum, C. F., Manganese Stabilizing Protein of Photosystem II Is a Thermostable, Natively Unfolded Polypeptide. *Biochemistry* **1999,** *38* (1), 404-414.

12. Popelkova, H.; Wyman, A.; Yocum, C., Amino acid sequences and solution structures of manganese stabilizing protein that affect reconstitution of Photosystem II activity. *Photosynth Res* **2003,** *77* (1), 21-34.

13. Uversky, V. N.; Gillespie, J. R.; Fink, A. L., Why are “natively unfolded” proteins unstructured under physiologic conditions? *Proteins: Structure, Function, and Bioinformatics* **2000,** *41* (3), 415-427.

14. Yamamoto, Y.; Doi, M.; Tamura, N.; Nishimura, M., Release of polypeptides from highly active O2-evolving photosystem-2 preparation by this treatment. *Febs Letters* **1981,** *133* (2), 265-268.

15. Ono, T.-A.; Inoue, Y., Mn-preserving extraction of 33-, 24-and 16-kDa proteins from O2-evolving PS II particles by divalent salt-washing. *FEBS letters* **1983,** *164* (2), 255-260.

16. Franzén, L.-G.; Hansson, Ö.; Andréasson, L.-E., The roles of the extrinsic subunits in Photosystem II as revealed by EPR. *Biochimica et Biophysica Acta (BBA)-Bioenergetics* **1985,** *808* (1), 171-179.

17. Miyao, M.; Murata, N., Role of the 33-kDa polypeptide in preserving Mn in the photosynthetic oxygen-evolution system and its replacement by chloride ions. *FEBS letters* **1984,** *170* (2), 350-354.

18. Bricker, T. M.; Frankel, L. K., The structure and function of the 33 kDa extrinsic protein of Photosystem II: A critical assessment. *Photosynthesis Research* **1998,** *56* (2), 157-173.

19. Svensson, B.; Tiede, D. M.; Nelson, D. R.; Barry, B. A., Structural studies of the manganese stabilizing subunit in photosystem II. *Biophysical journal* **2004,** *86* (3), 1807-1812.

20. Betts, S. D.; Hachigian, T. M.; Pichersky, E.; Yocum, C. F., Reconstitution of the spinach oxygen-evolving complex with recombinant Arabidopsis manganese-stabilizing protein. *Plant molecular biology* **1994,** *26* (1), 117-130.

21. Hutchison, R. S.; Betts, S. D.; Yocum, C. F.; Barry, B. A., Conformational Changes in the Extrinsic Manganese Stabilizing Protein Can Occur upon Binding to the Photosystem II Reaction Center: An Isotope Editing and FT-IR Study. *Biochemistry* **1998,** *37* (16), 5643-5653.

22. Kuwabara, T.; Murata, T.; Miyao, M.; Murata, N., Partial degradation of the 18-kDa protein of the photosynthetic oxygen-evolving complex: a study of a binding site. *Biochimica et Biophysica Acta (BBA)-Bioenergetics* **1986,** *850* (1), 146-155.

23. Glasoe, P. K.; Long, F., Use of glass electrodes to measure acidities in deuterium oxide1, 2. *The Journal of Physical Chemistry* **1960,** *64* (1), 188-190.

24. Busby, S. A.; Chalmers, M. J.; Griffin, P. R., Improving digestion efficiency under H/D exchange conditions with activated pepsinogen coupled columns. *International journal of mass spectrometry* **2007,** *259* (1-3), 130-139.

25. Hageman, T. S.; Weis, D. D., Reliable Identification of Significant Differences in Differential Hydrogen Exchange-Mass Spectrometry Measurements Using a Hybrid Significance Testing Approach. *Anal Chem* **2019,** *91* (13), 8008-8016.

26. Krissinel, E.; Henrick, K. In *Detection of protein assemblies in crystals*, International Symposium on Computational Life Science, Springer: 2005; pp 163-174.

27. Umena, Y.; Kawakami, K.; Shen, J. R.; Kamiya, N., Crystal structure of oxygen-evolving photosystem II at a resolution of 1.9 A. *Nature* **2011,** *473* (7345), 55-60.

28. Bricker, T. M.; Roose, J. L.; Fagerlund, R. D.; Frankel, L. K.; Eaton-Rye, J. J., The extrinsic proteins of Photosystem II. *Biochim Biophys Acta* **2012,** *1817* (1), 121-42.

29. Xu, Q.; Nelson, J.; Bricker, T. M., *Biochim. Biophys. Acta* **1994,** *1188*.

30. Shutova, T.; Irrgang, K. D.; Shubin, V.; Klimov, V. V.; Renger, G., *Biochemistry 36, 6350−6358*. 1997.

31. Zhang, L. X.; Liang, H. G.; Wang, J.; Li, W. R.; Yu, T. Z., Fluorescence and Fourier-transform infrared spectroscopic studies on the role of disulfide bond in the calcium binding in the 33 kDa protein of Photosystem II. *Photosynth Res* **1996,** *48* (3), 379-84.

32. Ahmed A, T.-R. H. a. C. R., A quantitative secondary structure analysis of the 33 kDa extrinsic protein of Photosystem II by FTIR spectroscopy. *FEBS Lett* **1995,** *363*, 65-68.

33. Betts, S. D.; Hachigian, T. M.; Pichersky, E.; Yocum, C. F., Reconstitution of the spinach oxygen-evolving complex with recombinant Arabidopsis manganese-stabilizing protein. *Plant Mol Biol* **1994,** *26* (1), 117-30.

34. Seidler, A.; Michel, H., Expression in Escherichia coli of the psbO gene encoding the 33 kd protein of the oxygen-evolving complex from spinach. *The EMBO journal* **1990,** *9* (6), 1743-1748.

35. Jensen P.F., R. K. D., Hydrogen exchange: A sensitive analytical window into protein conformation and dynamics. In *Hydrogen exchange mass spectrometry of proteins:Fundamentals, Methods, and Applications*, Weis, D. D., Ed. John Wiley & Sons: 2016; pp 1-26.

36. Fang, J.; Rand, K. D.; Beuning, P. J.; Engen, J. R., False EX1 signatures caused by sample carryover during HX MS analyses. *Int J Mass Spectrom* **2011,** *302* (1-3), 19-25.

37. Majumdar, R.; Manikwar, P.; Hickey, J. M.; Arora, J.; Middaugh, C. R.; Volkin, D. B.; Weis, D. D., Minimizing carry-over in an online pepsin digestion system used for the H/D exchange mass spectrometric analysis of an IgG1 monoclonal antibody. *Journal of the American Society for Mass Spectrometry* **2012,** *23* (12), 2140-2148.

38. Hutchison, R. S.; Betts, S. D.; Yocum, C. F.; Barry, B. A., *Biochemistry 37, 5643−5653*. 1998.

39. Berthold, D. A.; Babcock, G. T.; Yocum, C. F., *FEBS Lett.* **1981,** *134*.

40. Betts, S. D.; Hachigian, T. M.; Pichersky, E.; Yocum, C. F., *Plant Mol. Biol. 26, 117−130*. 1994.

41. Yamamoto, Y., Quality control of photosystem II. *Plant and Cell Physiology* **2001,** *42* (2), 121-128.

42. Virgin, I.; Ghanotakis, D. F.; Andersson, B., Light-induced D1-protein degradation in isolated photosystem II core complexes. *FEBS letters* **1990,** *269* (1), 45-48.

43. Aro, E.-M.; Hundal, T.; Carlberg, I.; Andersson, B., In vitro studies on light-induced inhibition of photosystem II and D1-protein degradation at low temperatures. *Biochimica et Biophysica Acta (BBA)-Bioenergetics* **1990,** *1019* (3), 269-275.

44. Mattoo, A. K.; Hoffman-Falk, H.; Marder, J. B.; Edelman, M., Regulation of protein metabolism: coupling of photosynthetic electron transport to in vivo degradation of the rapidly metabolized 32-kilodalton protein of the chloroplast membranes. *Proceedings of the National Academy of Sciences* **1984,** *81* (5), 1380-1384.

45. Ohad, I.; Kyle, D.; Arntzen, C., Membrane protein damage and repair: removal and replacement of inactivated 32-kilodalton polypeptides in chloroplast membranes. *The Journal of cell biology* **1984,** *99* (2), 481-485.

46. Hashimoto, A.; Akasaka, T.; Yamamoto, Y., Characteristics of the assembly of the 33 kDa oxygen-evolving complex protein in the etioplasts and the developing chloroplasts of barley seedlings. *Biochimica et Biophysica Acta (BBA)-Bioenergetics* **1993,** *1183* (2), 397-407.

47. Akiko, H.; Yasusi, Y.; Theg, S. M., Unassembled subunits of the photosynthetic oxygen-evolving complex present in the thylakoid lumen are long-lived and assembly-competent. *FEBS Letters* **1996,** *391* (1-2), 29-34.

Chapter 3

Structural analysis of engineered RTA* (RTA*-SS1) and RTA* by hydrogen exchange-mass spectrometry

3.1 Introduction

Ricin is extremely toxic plant protein produced as a byproduct from castor bean (*Ricinus communis)*. Ricin is lethal poison and documented as ribosomal inactivating protein.[1] Ricin is a bio threat and can be used for bioterrorism, because trace amount of ricin toxin can kill a human.[2] Recently NATO's biomedical advisory council ranked ricin toxin as number one potential bioweapon threat.[3] In USA, ricin is considered as category B bioterrorism agent by Centers for diseases Control and Prevention (https://emergency.cdc.gov/agent/agentlist-category.asp). It is high priority to develop a vaccine against ricin exposure for military and civilian.[4]

Ricin toxin (RT) is a heterodimer comprised of two ~30 kDa subunits, RTA and RTB.[5] RTA does the catalytic activity to inactivate mammalian ribosome function and shows cytotoxicity. The development of recombinant RTA vaccine is ongoing. Two RTA vaccine candidates, RiVax and RVEc, have been in development for a long time. RVEc was found as thermostable, nontoxic and immunogenic in a mouse model.[6-8] The RiVax antigen, referred to as RTA*, has two point mutations chosen to remove the enzymatic activity (Y80A) and prevent from vascular leak syndrome (V76M).[9] Structural studies of RiVax confirmed the minimal perturbation of tertiary structure occurs compared to native RTA.[10] RiVax protected mice against ricin challenge, but RiVax did not produce high titers of protective antibodies in humans.[11] While RiVax and RVEc showed some encouraging results in terms of safety and immunogenicity, the short half-life of toxin-specific antibodies and ineffective toxin neutralizing activity in human limits the potential of these two vaccines candidates.

The folded form of RTA has three domains.[5, 12] Folding domain I, residues (1-117) is comprised of six β-sheet and terminated with an α-helix known as α-helix B (residues 97–108). The α-helix B is considered a hotspot for binding of neutralizing antibodies.[13-15] Even though α-

helix B is a hotspot for binding for antibodies, still the RiVax vaccine fails to stimulate neutralizing antibodies in humans.[16] The α-helix B is a solvent-exposed secondary structural element that is connected by two loops at both ends of the main structure. Since α-helix B is a binding hotspot, flexible, and solvent-exposed, it might be possible to increase the rigidity of α-helix B by introducing a disulfide linkage. Our hypothesis is that flexibility of α-helix B affects the immunogenicity, and that increasing its rigidity could improve the antigen's potential to stimulate production of antibodies with higher toxin-neutralizing activity.

To test the rigidity-immunogenicity hypothesis, RTA* was engineered with two point mutations, A90C and F108C (referred to as RTA*-SS1) to add a disulfide linkage in α-helix B. These two cysteines are located on a loop that connects α-helix B with β-strand h (C90) and on β-strand g as the terminal residues of α-helix B (C108), so that two cysteines can form a disulfide bridge. After successful insertion of disulfide bond in RTA*-SS1 between residues 90 and 108, we were interested in comparing the higher-order structure of RTA* with RTA*-SS1. Here, we report the comparative structural studies of RTA* and RTA*-SS1 based on differential hydrogen exchange mass spectrometry (HX-MS).

3.2 Material & Methods

3.2.1 Materials

RTA* and RTA*-SS1 were received from the New York Structural Biology Center in HEPES buffer (20 mM HEPES, 150 mM NaCl, 20 mM imidazole, pH 7.5). Both of the samples were dialyzed into HEPES buffer without imidazole (20 mM HEPES, 150 mM NaCl, pH 7.5 in water) (Slide-A-Lyzer Dialysis Cassettes, ThermoFisher Scientific, 2000 Da MWCO, 3-12 mL). The masses of RTA*, RTA*-SS1, and reduced RTA*-SS1, determined by mass spectrometry, matched the theoretical masses within ±0.1 Da (**Figure 3.1a, 3.1b**). When RTA*-SS1 was reduced

with 0.5 M TCEP•HCl to confirm the engineered disulfide linkage, the mass of reduced RTA*-SS1 matched the theoretical mass within ±0.31 Da (**Figure 3.1c**). Increased mass of RTA*-SS1 from nonreduced form to reduced form confirms the disulfide linkage. The mass spectra of RTA* and RTA*-SS1 also show two peak at -27 Da and -54 Da relative to the major peak. We are unable to assign these two peaks, however, these peaks are not a problem since both samples contain the same peaks at similar abundance. The N-terminal of RTA* and RTA*-SS1 have four extra residues (-SNAM-) that are not part of the RTA native sequence. Therefore, sequence numbering of RTA* and RTA*-SS1 starts at (-3) serine, asparagine (-2), alanine (-1), and methionine (0), so that the residue 1 of RTA* and RTA*-SS1 match the native sequence numbering.

3.2.2 HX-MS measurements

For peptide-level HX-MS experiments, stocks of RTA* and RTA*-SS1 were diluted to 12 µM in 20 mM HEPES, 150 mM NaCl, pH 7.5 in water. Deuterium labelling was conducted by a robotic liquid handler (HDX PAL, LEAP Technologies, Carrboro, North Carolina). During the labelling experiment, 4 µL of each sample was diluted in 36 µL of protein buffer in D_2O (20 mM HEPES,150 mM NaCl, pD 7.5, pH was corrected for isotopic effect[17]) and labeled for 20 s, 102 s, 520 s, 2653 s, 13530 s and 69003 s with three replicates at 25 °C before LC-MS analysis. After labelling, 35 µL of labeled sample was quenched by 35 µL of quench buffer (200 mM glycine and 0.5 M TCEP•HCl at pH 2.5) at 0°C.

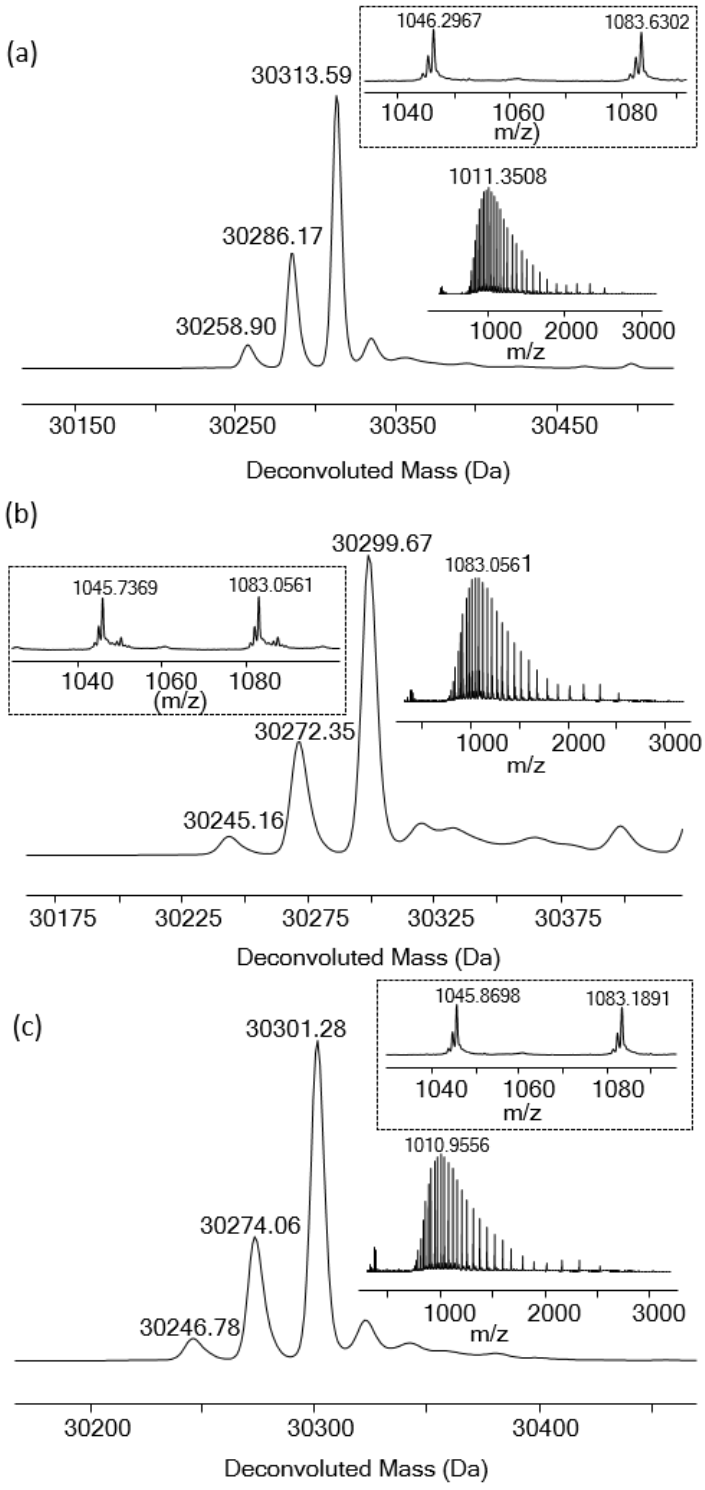

Figure 3.1. Deconvoluted mass spectrum with inlaid full and zoomed raw mass spectrum (a) RTA* (b) RTA*-SS1 (c) reduced RTA*-SS1. The theoretical masses were 30313.6 Da, 30299.6 Da, and 30301.6 Da, respectively

3.2.3 LC-MS analysis

Peptides from RTA* and RTA*-SS1 were generated by digestion with an immobilized pepsin column that was prepared in-house.[18] All peptides were trapped by a C-8 guard cartridge (Zorbax stable bond 300 C8, 2.1 x 12.5 mm, 5 µm particles) and separated by a C-18 column (Zorbax 300SB 2.1 × 50 mm, 3.5 µm particle diameter, Agilent, Santa Clara, CA) using an Agilent 1260 series (Santa Clara, CA) LC system. Mobile phase A was 0.1% formic acid in water, and mobile phase B was 0.1% formic acid in acetonitrile (gradient 13%-35%B over 10 minutes) with flow rate 200 µL/min.

3.2.4 Peptide mapping

Peptide mapping of RTA* was previously done by tandem mass spectrometry by our group.[19] In this project, RTA* was digested by pepsin and the resultant peptides were identified by mass (±3 ppm) and retention time matching (±0.4 min). RTA*-SS1 was also digested to map the same peptides found in RTA* other than mutation site. Mutation site peptide was confirmed by MSMS. **Figure 3.2** shows a precursor (ITHLCT, m/z: 344.1793) with matched product ions y_1, y_2, y_4-H_20, y_5, b_3, etc) confirmed the mutation site peptide. All MSMS confirmed peptides that were identified in this project are mapped in **Figure. 3.3**.

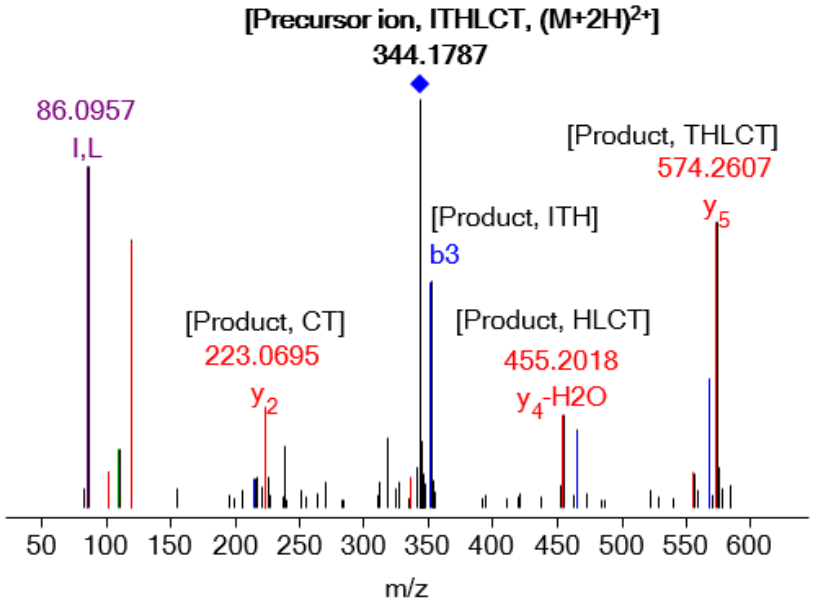

Figure 3.2. MSMS spectrum of mutant peptide: ITHLCT (RTA*-SS1).

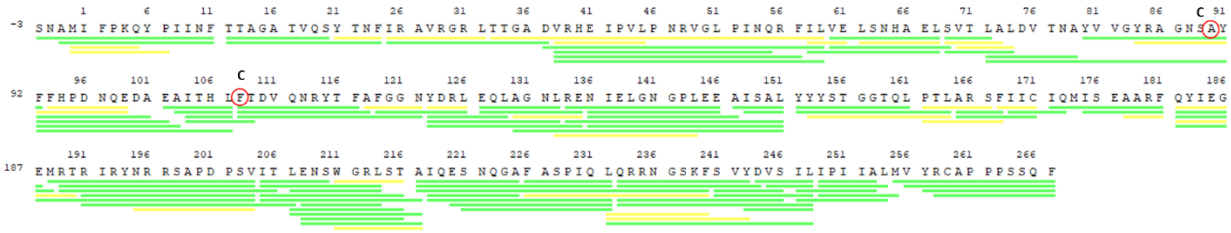

Figure 3.3. RTA* peptide coverage map.

3.2.5 Data analysis

A total of 125 peptides with 100% sequence coverage were analyzed using Sierra Analytics HDExaminer (Sierra Analytics, Modesto, CA). We have overlapping peptides across the protein sequence to further validate our HX-MS results. HDExaminer was also used for hybrid significance testing.[20] In HDExaminer, each peptide with high quality mass spectra in a single charge state was chosen to represent HX-MS data for the peptide. Spectra were manually checked and verified for all replicates. For each peptide, deuterium uptake was calculated by the difference between the centroid mass of deuterated peptide in each labelling time point with centroid mass of undeuterated control. The chemical exchange rate was calculated on H to D exchange from the spreadsheet given in (http://hx2.med.upenn.edu/download.html). [21, 22] The backbone flexibility of RTA* was calculated from the following equation:

$$\text{flexibility (\%)} = \frac{\Delta m}{\Delta m 69000s} \times 100\% \quad (1)$$

Where Δm is the deuterium uptake at 20 s, and Δm_{69000s} is the deuterium uptake at highest labeling time point in our experiment. Further, these data were categorized by k-means clustering into three different categories: rigid, intermediate, and flexible using an R script (**see Appendix B**). In the mapping of the flexibility categories onto the RTA*-SS1 structure, when partially overlapping peptides were assigned to flexible and intermediate categories, the overlapping region was mapped as flexible when partially overlapping peptides were assigned to rigid and intermediate categories, the overlapping region was mapped as rigid, and when partially overlapping were assigned to rigid and flexible categories, the overlapping region was classified as conflicting.

3.3 Results and discussion

3.3.1 Design strategy of engineered version of RTA* at α-helix B

While mutant enzymatic subunit RTA* looked promising in a pre-clinal studies, RTA* failed to stimulate toxin-neutralizing antibodies in clinical trials.[11] Ricin enzymatic unit, RTA, has four different epitope regions for antibody binding, clusters I-IV. Out of four clusters, cluster I (α-helix B, residues 97-108) was found to be promising because α-helix B is a binding hotspot for neutralizing antibodies. [13-15, 23] So it was hypothesized that stabilizing α-helix B would make RTA* more immunogenic. The α-helix B (residues 97-108) is a solvent-exposed helix joined by β-strand g and h and connecting loops. RTA*-SS1 was engineered to stabilize helix B by inserting a disulfide linkage. According to that idea, 108F located on β-strand g as the terminal residue of α-helix B and the nearest residue 90Y located on a loop that connect α-helix B with β-strand h were selected for mutation. In this work, we wanted to see how the mutations affected the higher-order structure of RTA*-SS1 compared to RTA*. Our expectation was that the disulfide bond would stabilize the α-helix B, and in HX-MS, we would see slower HX kinetics in RTA*-SS1 compared to RTA*.

3.3.2 HX-MS results of RTA* to describe the backbone of their structure

The degree of flexibility in RTA* was classified based on fractional hydrogen exchange measured at 20 s (see equation 1). The fractional exchange data were classified into three categories by k-means clustering: rigid, intermediate and flexible. **Figure 3.4** shows the structural categories of RTA*. In **Figure 3.4(a)** the peptide index numbers the peptides from N-terminal to C-terminal.

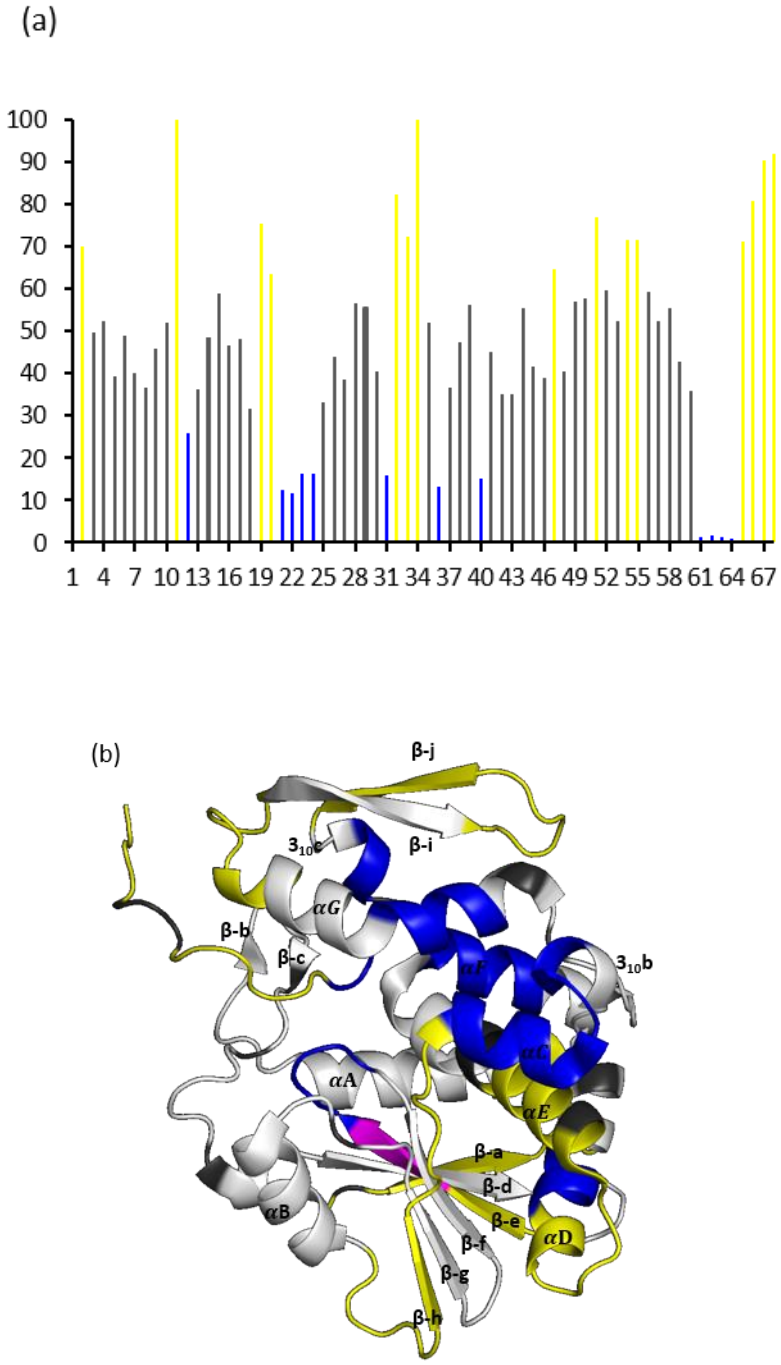

Figure 3.4. (a) Relative flexibility of RTA* determined by k-means clustering (b) The flexibility categories mapped onto the structure of RTA* (PDB 3SRP). The color categories correspond to colors depicted in a.

Figure 3.4b shows the flexible and rigid regions of RTA* structure. The flexible regions (colored in yellow) are located in residues –3-20 (α-helix A and β-strand a), 69-71 (β-strand e), 108-122 (β-strand h connecting loop to α-helix C), 152-171 (α-helix D and α-helix E), 218-225 (α-helix G connecting loop to β-sheet i), 233-244 (β-strand I to β-strand j), and 255-267 (loop coming from 3_{10}c to c terminal). The rigid regions of RTA* (colored in blue) are located in residues 75-79 (connecting loop of β-strand e and β-strand f), 123-135 (α-helix C and 3_{10}b), 147-151 (α-helix D), 182-188 (α-helix F), 205-210 (α-helix G) and 247-254 (3_{10}c). The residues that do not fall under the categories of flexible and rigid are classified as intermediate and are shown in gray (**Fig. 3.4b**). The purple color region is assigned as conflicting because the residues of overlapping peptides were classified as flexible and rigid.

3.3.3 Comparison of HX of RTA*-SS1 and RTA*

To investigate the effect of inserting a disulfide linkage in α-helix B (residues 97-108), we measured HX differences between RTA*-SS1 and RTA* at HX labeling times between 20 and 69003 s. Any positive quantity in HX difference means faster HX rate caused by addition of the disulfide in helix B, i.e. deprotection from HX, and any negative quantity means slower HX rate, or protection from HX, caused by the additional disulfide bond. Representative HX uptake plots are shown in **Figure 3.5a**. Hybrid significance testing, represented by a volcano plot, was used to identify statistically significant HX differences at 99% confidence interval (**Figure 3.6**). **Figure 3.7** shows the visualization of the significant HX results on RTA*-SS1 structure. Comparison of HX-MS data of RTA* and RTA*-SS1 revealed regions where the addition of the disulfide bond in helix B caused statistically significant changes in HX rate. The blue regions show the protected regions and yellow regions show the deprotected regions. A total of 11 peptides showed subtle but

statistically significant differences between RTA*-SS1 and RTA* (**Appendix B, Figure 3.B-1 and Figure 3.B-2**).

HX protection was found in only one region, covered by two peptides **(Appendix B, Figure 3.B-1**), that was caused by the addition of the disulfide bond. The protected region is residues 217-248 (the proximal end of α helix G connected through a loop to β strands i and j and the 3_{10} helix c). In wild-type RTA*, residues 217-248 are flexible (α helix G connected through a loop to β strand i and β-strand j), intermediate region (β strand i) and rigid (3_{10} helix c) (folding domain III, **Figure 3.4a**). Addition of the disulfide bond caused statistically significant deprotection in residues -3-11 (β-stand a, folding domain I), 37-59 (β-strand b,c, and d and 3_{10}a, folding domain I), 72-91 (β-strand e, f, and g, folding domain I), 108-118 (β-strand h, folding domain I) and 123-135 (3_{10}b, α-helix C, folding domain II). Regions -3 to 11 of RTA* is flexible (folding domain I). Region 37 to 59 is flexible and intermediate (folding domain I). Region 72 to 91 is intermediate with part of β-strand e is rigid and three residues have conflicting assignments (folding domain I). Region 108 to 118 is flexible (folding domain I). Region 123 to 135 is rigid (folding domain II). Deprotected regions are mostly in the vicinity of the added disulfide bond and located in folding domain I. Folding domain II is nearly unaffected by the mutation except 3_{10}b, α-helix C region. All of the regions that became protected by addition of the disulfide bond are in folding domain III.

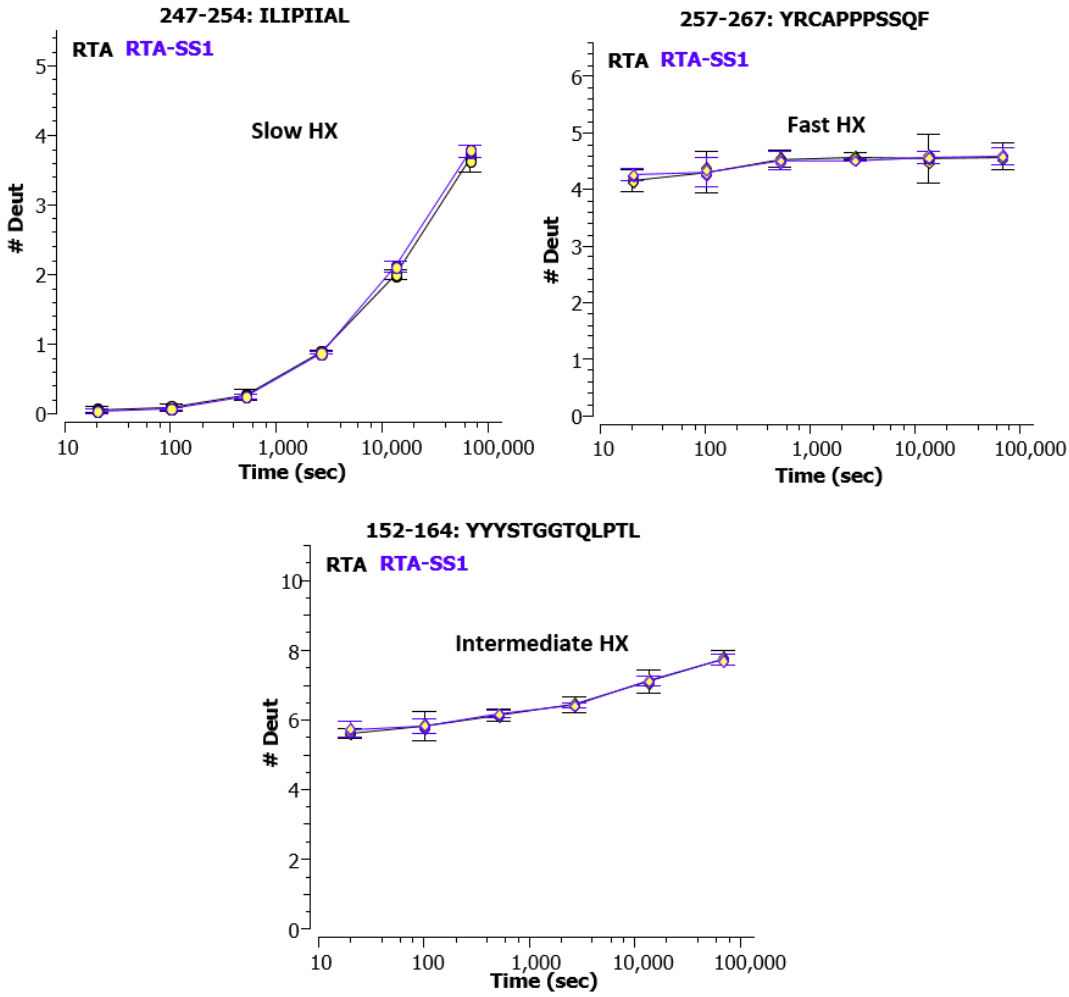

Figure 3.5. Representative deuterium uptake plots for slow, fast, and intermediate HX.

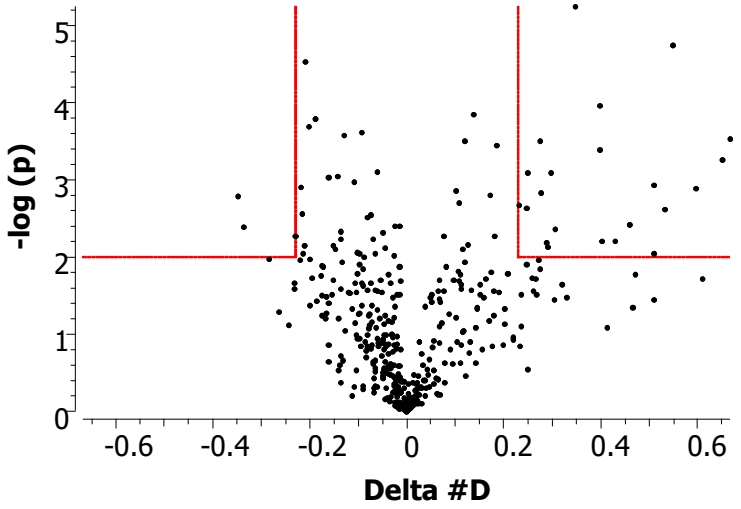

Figure 3.6. Hybrid significance testing of HX differences between RTA*-SS1 and RTA* represented by a volcano plot. The significance criteria are $p < 0.01$ (red solid lines) and $|\Delta D| > 0.223$ Da.

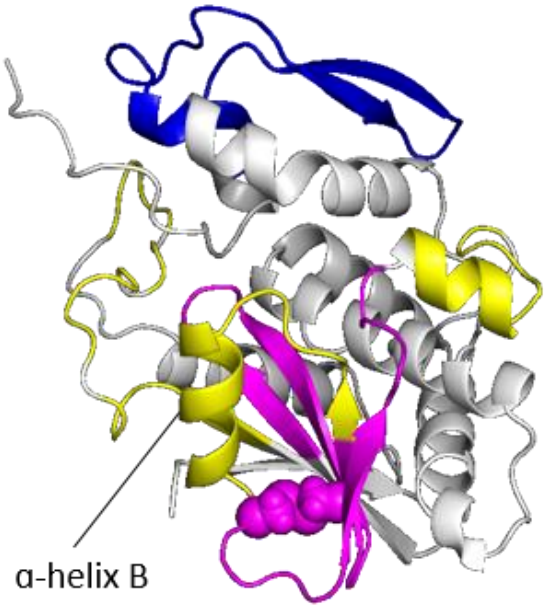

Figure 3.7. HX results on RTA*-SS1 structure. X-ray crystal structure of RTA*-SS1 has been solved, M. Rudolph et al., manuscript in preparation. The disulfide bond is shown in space-filling representation. Regions colored yellow denotes faster HX by RTA*-SS1, regions colored blue denote slower HX by RTA*-SS1. Magenta denotes mutant peptides. Pymol was used to visualize the HX-MS results.

3.3.4 Addition of disulfide bond in helix B also alters chemical HX rate

To compare the HX kinetics of the peptides in RTA*-SS1 with the mutations to peptides from the same locations in RTA*, we need to consider the fundamentals of HX. According to the Linderstrøm-Lang model[23, 24] of HX, protein breathing motions in solution cause conformational fluctuations that occur for a very short amount time. These transient structural fluctuations allows the protein backbone to open its amide hydrogen bonds to permit exchange with deuterium. The rate of hydrogen exchange depends on the ratio of the rate of opening and closing and also on the unique rate of chemical exchange of each amide (**see chapter 1: section 1.1.2**). In general, HX comparisons can only be made when chemical exchange is constant between protein states. However, for a structural comparison of protein states with differences in amino acid sequence, hydrogen exchange rate differences depend on both conformational dynamics and also chemical exchange as chemical rate depends on sequence. Since we have mutation on RTA*-SS1, we must consider both conformational differences and chemical exchange differences, therefore we have calculated the rate constants for chemical exchange of the residues at and near the mutation sites, and compared with RTA*(**Figure 3.8**). Our calculation shows the chemical HX rate constant is substantially faster after mutation in residues 90, 91, 107 and 108 with magnitude of ~4-10-fold faster (**Figure 3.8**). Our HX results for peptides covering the mutation sites also show significantly faster HX in RTA*-SS1. Comparison of HX-MS of RTA* and RTA*-SS1 in the mutant site is complicated, because HX rate depends on both the conformational dynamics and chemical exchange. Thus, our HX results at the mutation site are inconclusive here to determine the

stabilization or destabilization of α-helix B, because the observed HX changes could be due to chemical exchange rate or conformational/dynamical factor.

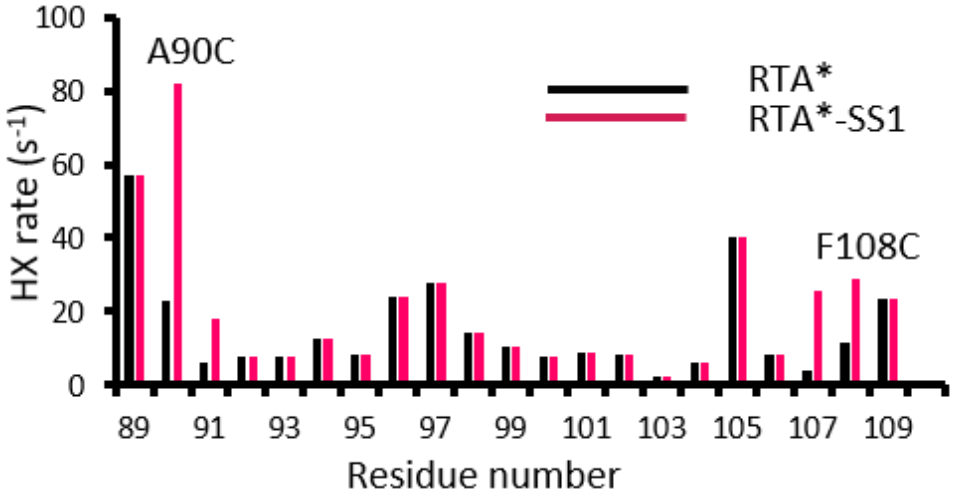

Figure 3.8. Chemical exchange rate in for RTA* and RTA*-SS1.

3.3.5 Engineered RTA* design strategy vs experimental outcome

In this study, we used the HX-MS technique to compare the structural dynamics of RTA* and RTA*-SS1 in order to determine if putting a disulfide linkage between 90 and 108 positions in α-helix B site could be an approach to increase the immunogenicity of RTA*.

After confirming, by peptide mapping, the mutated version of RTA*, in HX, the expected outcome was to see the slower hydrogen exchange in RTA*-SS1 near the mutation site. Our current HX results (faster HX) cannot to be used to make any conclusion about α-helix B, because of the faster HX observed in the mutation site could be due to faster, slower, or unchanged structural dynamics combined with faster chemical HX (**Figure 3.8**). Our HX-MS data statistically showed both protection (folding domain III) and deprotection (folding domain I and slightly in II) in RTA*-SS1 structure as a result of disulfide bond inclusion. Overall mutation alter some of the structural parts of RTA*-SS1 subtly, but does not drastically change the structure.

3.4 Appendix B

R Script:

```
getwd()
setwd("C:/Users/h149h941/Documents")
setwd("C:/Users/h149h941/Documents/R_RTA_RTA_SS1")
HX_data<read.csv("RTA.csv")
HX_data<-read.csv("RTA.csv")
HX_data
HX_data$X.D.Corr.
kmeans((HX_data$X.D.Corr.),3)$cluster
HX_data$HXcluster<-kmeans((HX_data$X.D.Corr.),3)$cluster
write.csv(HX_data, "clustered.csv", row.names = False)
write.csv(HX_data, "clustered.csv", row.names = FALSE)
q()
```

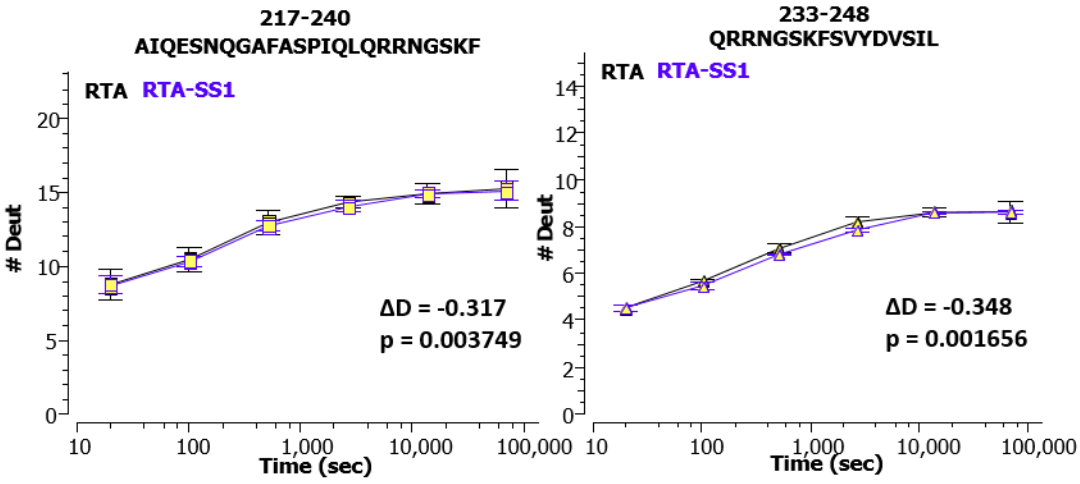

Figure 3.B-1. Deuterium uptake plots for statistically significant protection in RTA*-SS1.

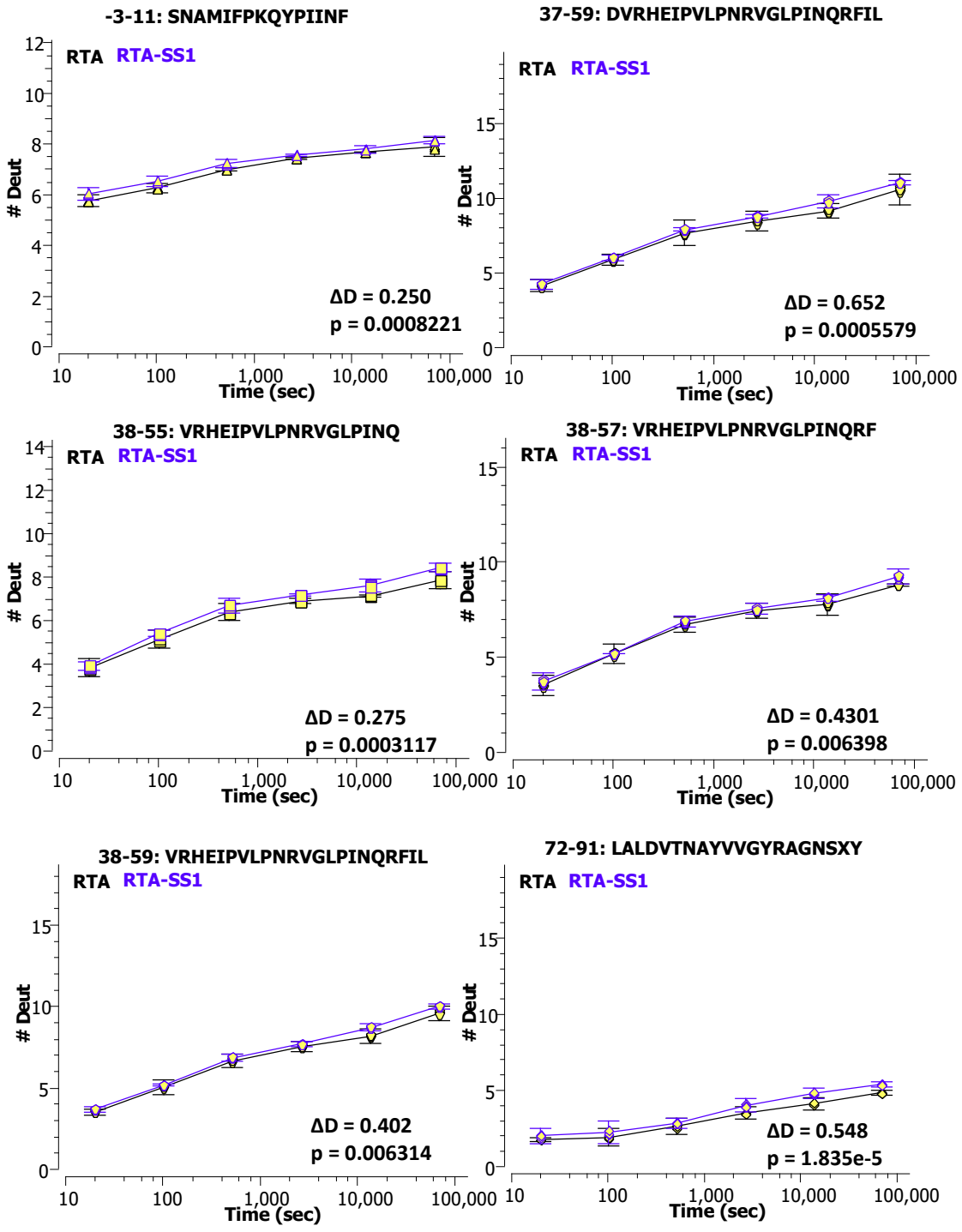
-3-11: SNAMIFPKQYPIINF
RTA RTA-SS1
Deut
ΔD = 0.250
p = 0.0008221
Time (sec)
37-59: DVRHEIPVLPNRVGLPINQRFIL
RTA RTA-SS1
Deut
ΔD = 0.652
p = 0.0005579
Time (sec)
38-55: VRHEIPVLPNRVGLPINQ
RTA RTA-SS1
Deut
ΔD = 0.275
p = 0.0003117
Time (sec)
38-57: VRHEIPVLPNRVGLPINQRF
RTA RTA-SS1
Deut
ΔD = 0.4301
p = 0.006398
Time (sec)
38-59: VRHEIPVLPNRVGLPINQRFIL
RTA RTA-SS1
Deut
ΔD = 0.402
p = 0.006314
Time (sec)
72-91: LALDVTNAYVVGYRAGNSXY
RTA RTA-SS1
Deut
ΔD = 0.548
p = 1.835e-5
Time (sec)

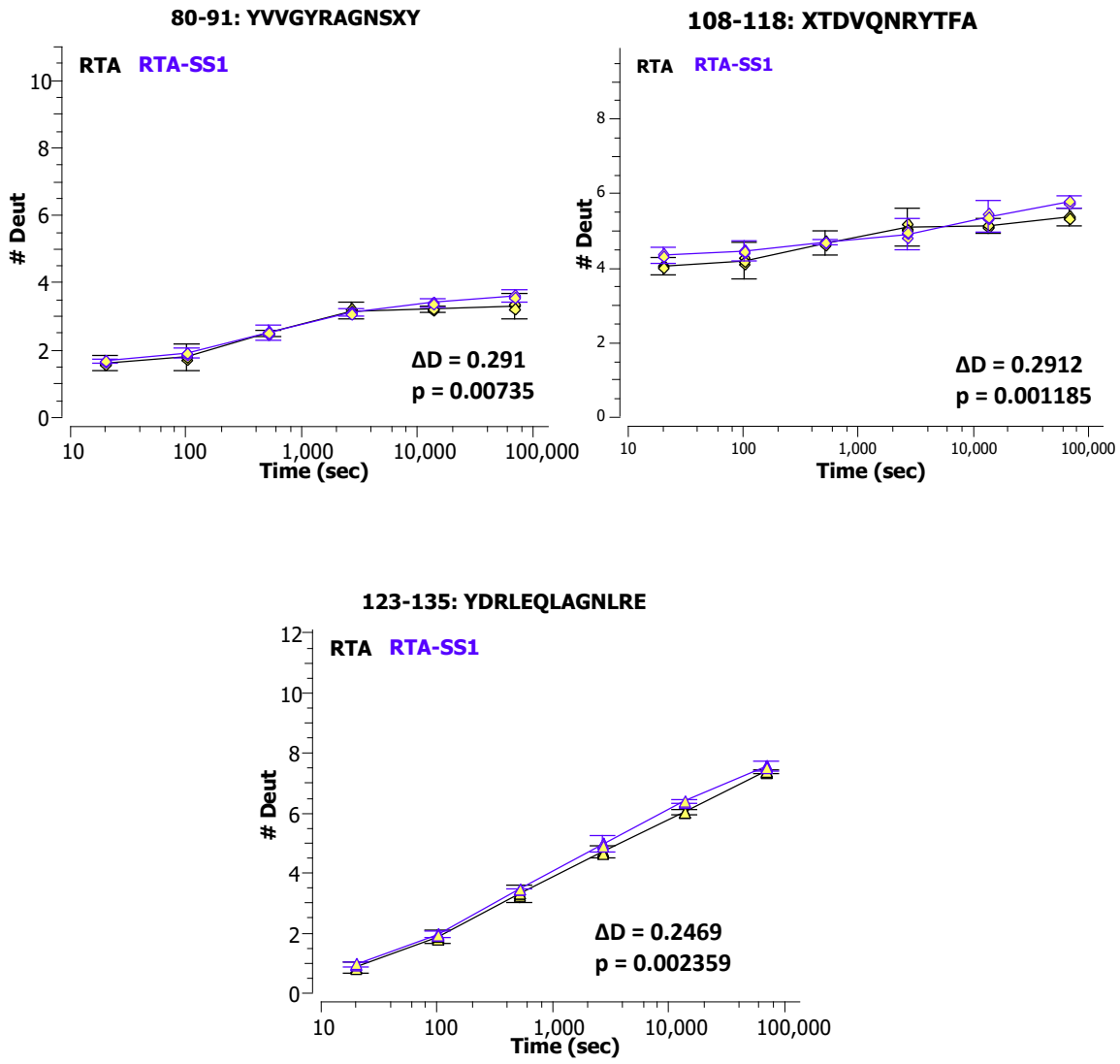

Figure 3.B-2. Deuterium uptake plots for statistically significant protection in RTA*-SS1.

3.5 References

1. Ballinger, M. J.; Perlman, S. J., Generality of toxins in defensive symbiosis: ribosome-inactivating proteins and defense against parasitic wasps in Drosophila. *PLoS pathogens* **2017,** *13* (7), e1006431.

2. Audi, J.; Belson, M.; Patel, M.; Schier, J.; Osterloh, J., Ricin poisoning: a comprehensive review. *Jama* **2005,** *294* (18), 2342-2351.

3. Cieslak, T. J.; Kortepeter, M. G.; Wojtyk, R. J.; Jansen, H.-J.; Reyes, R. A.; Smith, J. O.; Panel, N. B. M. A., Beyond the dirty dozen: a proposed methodology for assessing future bioweapon threats. *Military medicine* **2018,** *183* (1-2), e59-e65.

4. Reisler, R. B.; Smith, L. A., The need for continued development of ricin countermeasures. *Adv Prev Med* **2012,** *2012*, 149737.

5. Montfort, W.; Villafranca, J. E.; Monzingo, A. F.; Ernst, S. R.; Katzin, B.; Rutenber, E.; Xuong, N. H.; Hamlin, R.; Robertus, J. D., The three-dimensional structure of ricin at 2.8 A. *Journal of Biological Chemistry* **1987,** *262* (11), 5398-5403.

6. McLain, D. E.; Horn, T. L.; Detrisac, C. J.; Lindsey, C. Y.; Smith, L. A., Progress in Biological Threat Agent Vaccine Development: A Repeat-Dose Toxicity Study of a Recombinant Ricin Toxin A-Chain (rRTA) 1-33/44-198 Vaccine (RV Ec) in Male and Female New Zealand White Rabbits. *International journal of toxicology* **2011,** *30* (2), 143-152.

7. McLain, D. E.; Lewis, B. S.; Chapman, J. L.; Wannemacher, R. W.; Lindsey, C. Y.; Smith, L. A., Protective effect of two recombinant ricin subunit vaccines in the New Zealand white rabbit subjected to a lethal aerosolized ricin challenge: survival, immunological response, and histopathological findings. *Toxicological Sciences* **2012,** *126* (1), 72-83.

8. Roy, C. J.; Brey, R. N.; Mantis, N. J.; Mapes, K.; Pop, I. V.; Pop, L. M.; Ruback, S.; Killeen, S. Z.; Doyle-Meyers, L.; Vinet-Oliphant, H. S., Thermostable ricin vaccine protects rhesus macaques against aerosolized ricin: Epitope-specific neutralizing antibodies correlate with protection. *Proceedings of the National Academy of Sciences* **2015,** *112* (12), 3782-3787.

9. Smallshaw, J. E.; Firan, A.; Fulmer, J. R.; Ruback, S. L.; Ghetie, V.; Vitetta, E. S., A novel recombinant vaccine which protects mice against ricin intoxication. *Vaccine* **2002,** *20* (27-28), 3422-3427.

10. Legler, P. M.; Brey, R. N.; Smallshaw, J. E.; Vitetta, E. S.; Millard, C. B., Structure of RiVax: a recombinant ricin vaccine. *Acta Crystallographica Section D: Biological Crystallography* **2011,** *67* (9), 826-830.

11. Vitetta, E. S.; Smallshaw, J. E.; Coleman, E.; Jafri, H.; Foster, C.; Munford, R.; Schindler, J., A pilot clinical trial of a recombinant ricin vaccine in normal humans. *Proceedings of the National Academy of Sciences* **2006,** *103* (7), 2268-2273.

12. Rutenber, E.; Katzin, B. J.; Ernst, S.; Collins, E. J.; Mlsna, D.; Ready, M. P.; Robertus, J. D., Crystallographic refinement of ricin to 2.5 Å. *Proteins: Structure, Function, and Bioinformatics* **1991,** *10* (3), 240-250.

13. O'Hara, J. M.; Neal, L. M.; McCarthy, E. A.; Kasten-Jolly, J. A.; Brey III, R. N.; Mantis, N. J., Folding domains within the ricin toxin A subunit as targets of protective antibodies. *Vaccine* **2010,** *28* (43), 7035-7046.

14. O'Hara, J. M.; Kasten-Jolly, J. C.; Reynolds, C. E.; Mantis, N. J., Localization of non-linear neutralizing B cell epitopes on ricin toxin's enzymatic subunit (RTA). *Immunology letters* **2014,** *158* (1-2), 7-13.

15. Lemley, P. V.; AMANATIDES, P.; WRIGHT, D. C., Identification and characterization of a monoclonal antibody that neutralizes ricin toxicity in vitro and in vivo. *Hybridoma* **1994,** *13* (5), 417-421.

16. O'Hara, J. M.; Yermakova, A.; Mantis, N. J., Immunity to ricin: fundamental insights into toxin-antibody interactions. *Curr Top Microbiol Immunol* **2012,** *357*, 209-41.

17. Glasoe, P. K.; Long, F., Use of glass electrodes to measure acidities in deuterium oxide1, 2. *The Journal of Physical Chemistry* **1960,** *64* (1), 188-190.

18. Busby, S. A.; Chalmers, M. J.; Griffin, P. R., Improving digestion efficiency under H/D exchange conditions with activated pepsinogen coupled columns. *International journal of mass spectrometry* **2007,** *259* (1-3), 130-139.

19. Angalakurthi, S. K.; Vance, D. J.; Rong, Y.; Nguyen, C. M. T.; Rudolph, M. J.; Volkin, D.; Middaugh, C. R.; Weis, D. D.; Mantis, N. J., A Collection of Single-Domain Antibodies that Crowd Ricin Toxin's Active Site. *Antibodies (Basel)* **2018,** *7* (4).

20. Hageman, T. S.; Weis, D. D., Reliable Identification of Significant Differences in Differential Hydrogen Exchange-Mass Spectrometry Measurements Using a Hybrid Significance Testing Approach. *Anal Chem* **2019,** *91* (13), 8008-8016.

21. Nguyen, D.; Mayne, L.; Phillips, M. C.; Walter Englander, S., Reference parameters for protein hydrogen exchange rates. *Journal of The American Society for Mass Spectrometry* **2018,** *29* (9), 1936-1939.

22. Bai, Y.; Milne, J. S.; Mayne, L.; Englander, S. W., Primary structure effects on peptide group hydrogen exchange. *Proteins: Structure, Function, and Bioinformatics* **1993,** *17* (1), 75-86.

23. Hvidt, A.; Linderstrøm-Lang, K., Exchange of hydrogen atoms in insulin with deuterium atoms in aqueous solutions. *Biochimica et biophysica acta* **1954,** *14* (4), 574.

24. Englander, S.; Mayne, L.; Bai, Y.; Sosnick, T., Hydrogen exchange: the modern legacy of Linderstrøm-Lang. *Protein science* **1997,** *6* (5), 1101-1109.

Chapter 4: Appendix C

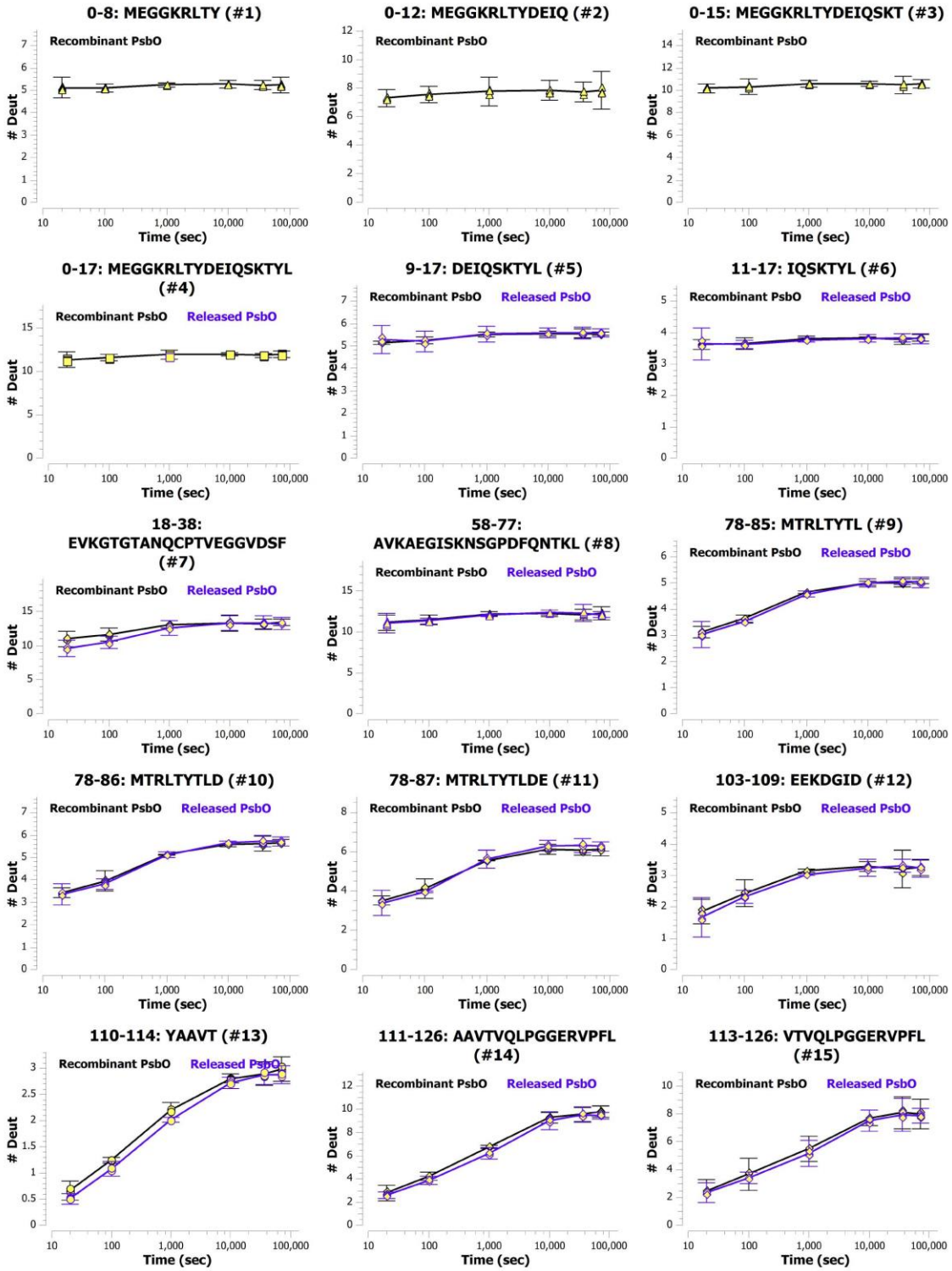
0-8: MEGGKRLTY (#1)
Recombinant PsbO
0-12: MEGGKRLTYDEIQ (#2)
Recombinant PsbO
0-15: MEGGKRLTYDEIQSKT (#3)
Recombinant PsbO
0-17: MEGGKRLTYDEIQSKTYL (#4)
Recombinant PsbO
Released PsbO
9-17: DEIQSKTYL (#5)
Recombinant PsbO
Released PsbO
11-17: IQSKTYL (#6)
Recombinant PsbO
Released PsbO
18-38: EVKGTGTANQCPTVEGGVDSF (#7)
Recombinant PsbO
Released PsbO
58-77: AVKAEGISKNSGPDFQNTKL (#8)
Recombinant PsbO
Released PsbO
78-85: MTRLTYTL (#9)
Recombinant PsbO
Released PsbO
78-86: MTRLTYTLD (#10)
Recombinant PsbO
Released PsbO
78-87: MTRLTYTLDE (#11)
Recombinant PsbO
Released PsbO
103-109: EEKDGID (#12)
Recombinant PsbO
Released PsbO
110-114: YAAVT (#13)
Recombinant PsbO
Released PsbO
111-126: AAVTVQLPGGERVPFL (#14)
Recombinant PsbO
Released PsbO
113-126: VTVQLPGGERVPFL (#15)
Recombinant PsbO
Released PsbO
Deut
Time (sec)
10
100
1,000
10,000
100,000

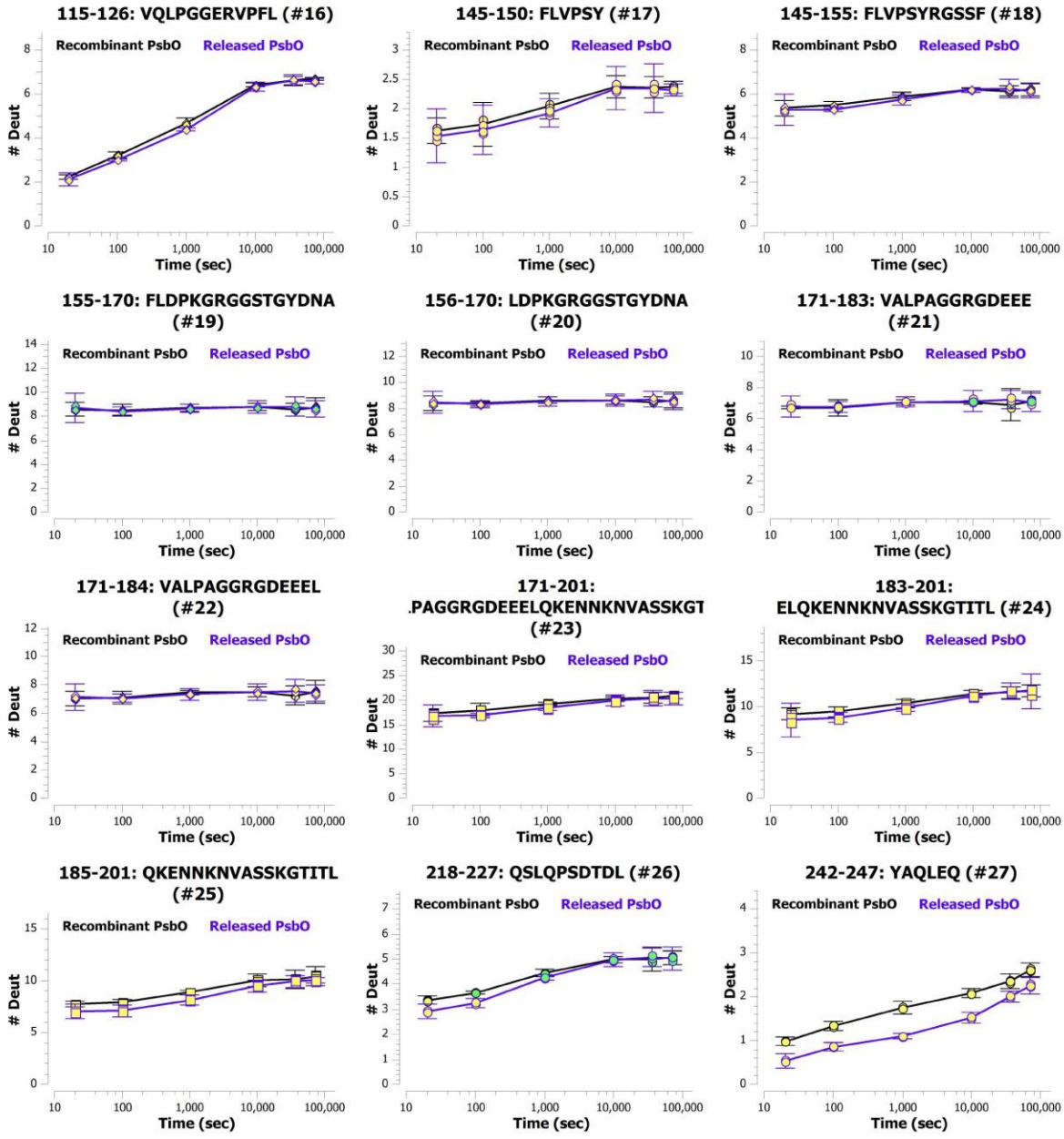

Figure 4.C-1. Deuterium uptake plots for recombinant PsbO (black color) and released PsbO (violet color).

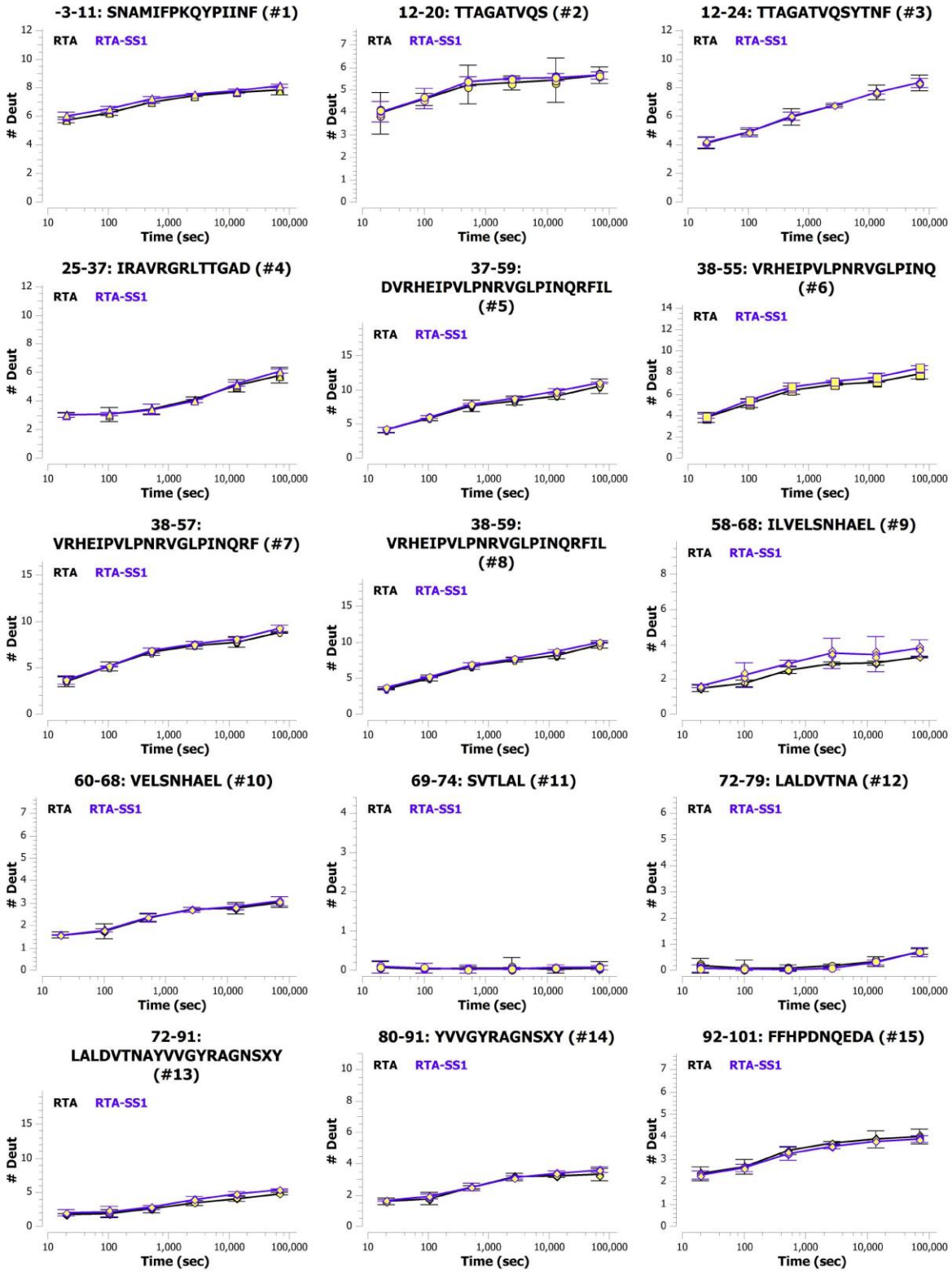
-3-11: SNAMIFPKQYPIINF (#1)
12-20: TTAGATVQS (#2)
12-24: TTAGATVQSYTNF (#3)
25-37: IRAVRGRLTTGAD (#4)
37-59: DVRHEIPVLPNRVGLPINQRFIL (#5)
38-55: VRHEIPVLPNRVGLPINQ (#6)
38-57: VRHEIPVLPNRVGLPINQRF (#7)
38-59: VRHEIPVLPNRVGLPINQRFIL (#8)
58-68: ILVELSNHAEL (#9)
60-68: VELSNHAEL (#10)
69-74: SVTLAL (#11)
72-79: LALDVTNA (#12)
72-91: LALDVTNAYVVGYRAGNSXY (#13)
80-91: YVVGYRAGNSXY (#14)
92-101: FFHPDNQEDA (#15)
RTA
RTA-SS1
Deut
Time (sec)
10
100
1,000
10,000
100,000

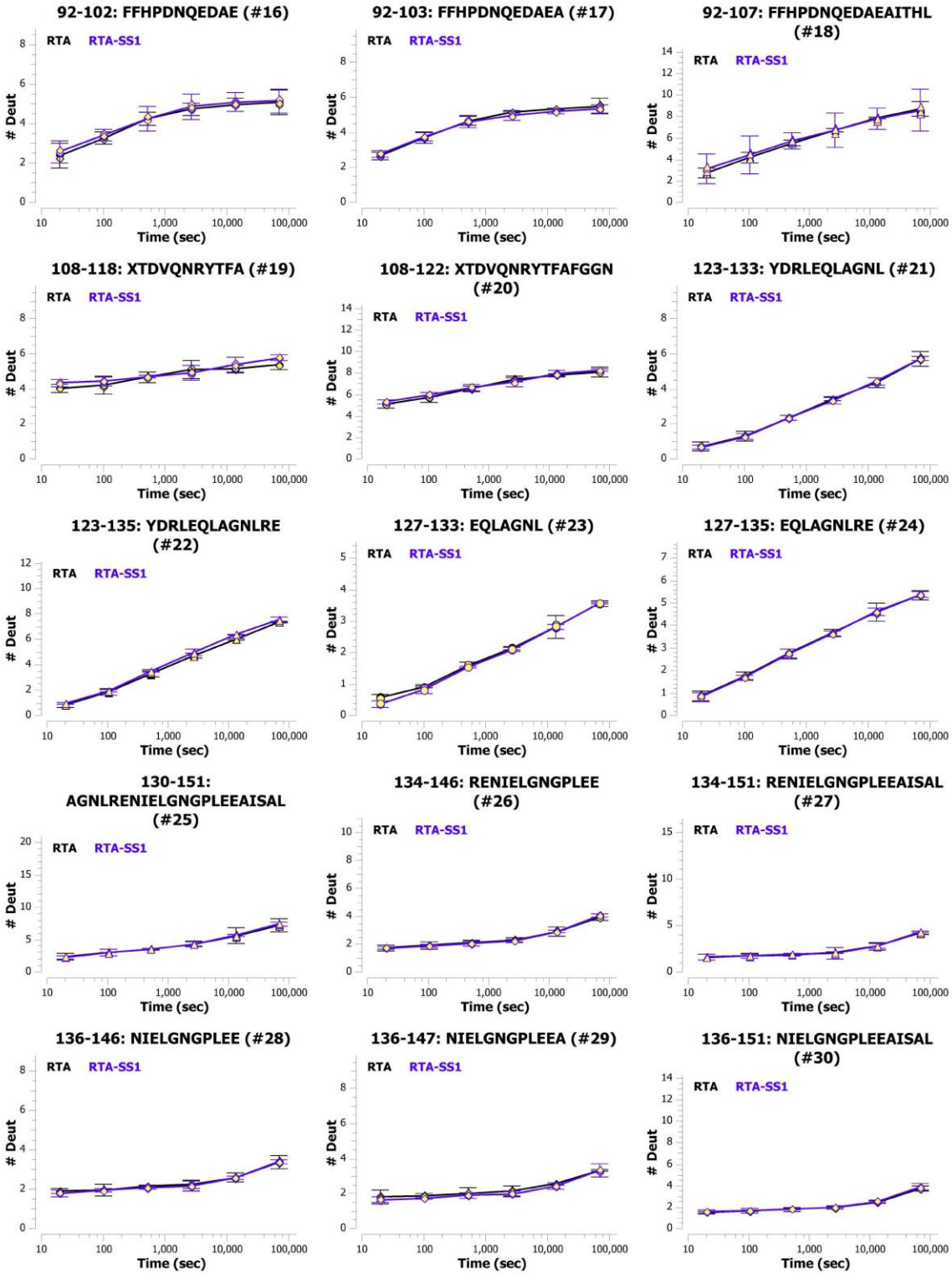
92-102: FFHPDNQEDAE (#16)
92-103: FFHPDNQEDAEA (#17)
92-107: FFHPDNQEDAEAITHL (#18)
108-118: XTDVQNRYTFA (#19)
108-122: XTDVQNRYTFAFGGN (#20)
123-133: YDRLEQLAGNL (#21)
123-135: YDRLEQLAGNLRE (#22)
127-133: EQLAGNL (#23)
127-135: EQLAGNLRE (#24)
130-151: AGNLRENIELGNGPLEEAISAL (#25)
134-146: RENIELGNGPLEE (#26)
134-151: RENIELGNGPLEEAISAL (#27)
136-146: NIELGNGPLEE (#28)
136-147: NIELGNGPLEEA (#29)
136-151: NIELGNGPLEEAISAL (#30)
RTA
RTA-SS1
Deut
Time (sec)
10
100
1,000
10,000
100,000

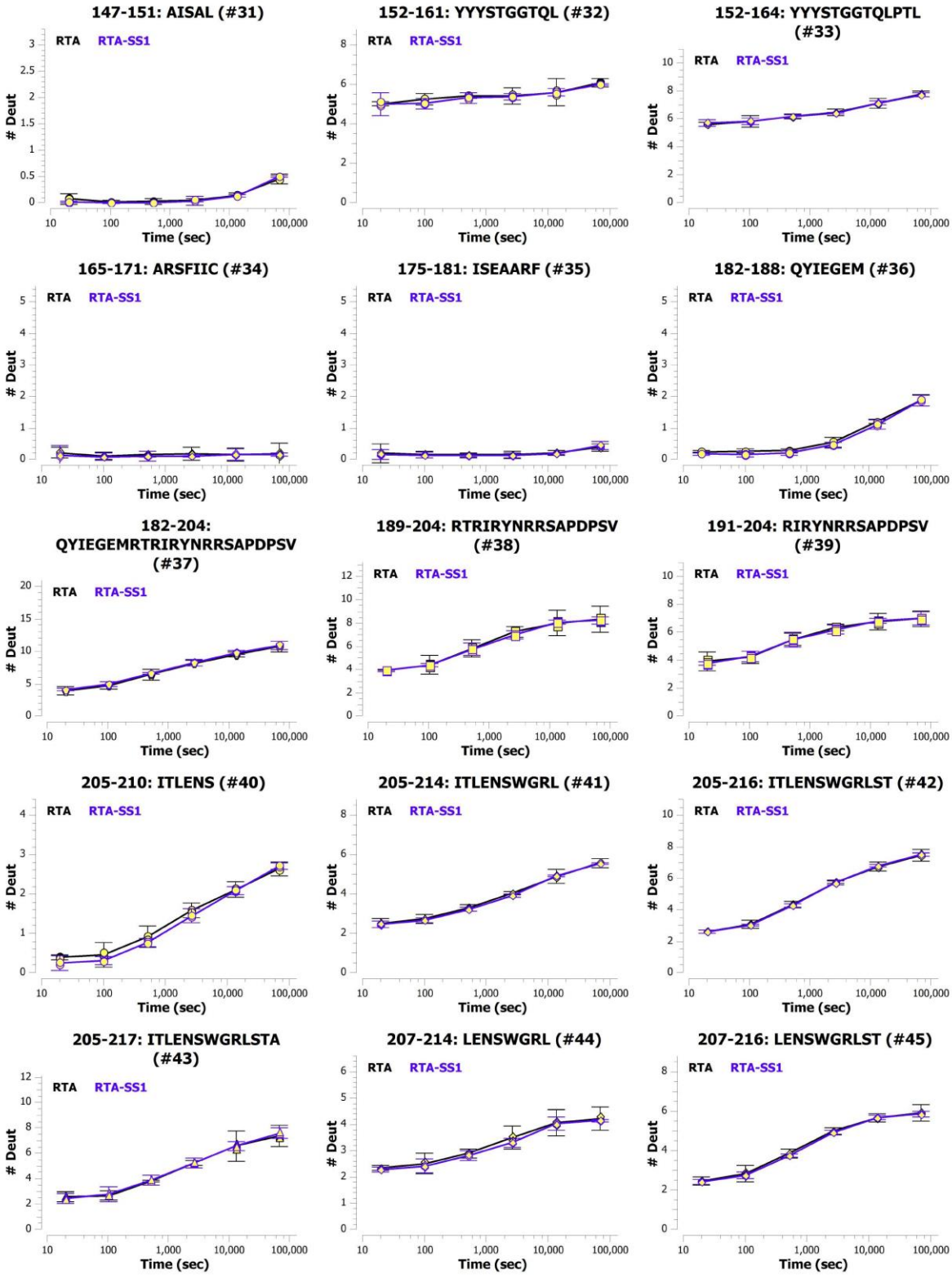
147-151: AISAL (#31)
152-161: YYYSTGGTQL (#32)
152-164: YYYSTGGTQLPTL (#33)
165-171: ARSFIIC (#34)
175-181: ISEAARF (#35)
182-188: QYIEGEM (#36)
182-204: QYIEGEMRTRIRYNRRSAPDPSV (#37)
189-204: RTRIRYNRRSAPDPSV (#38)
191-204: RIRYNRRSAPDPSV (#39)
205-210: ITLENS (#40)
205-214: ITLENSWGRL (#41)
205-216: ITLENSWGRLST (#42)
205-217: ITLENSWGRLSTA (#43)
207-214: LENSWGRL (#44)
207-216: LENSWGRLST (#45)
RTA
RTA-SS1
Deut
Time (sec)

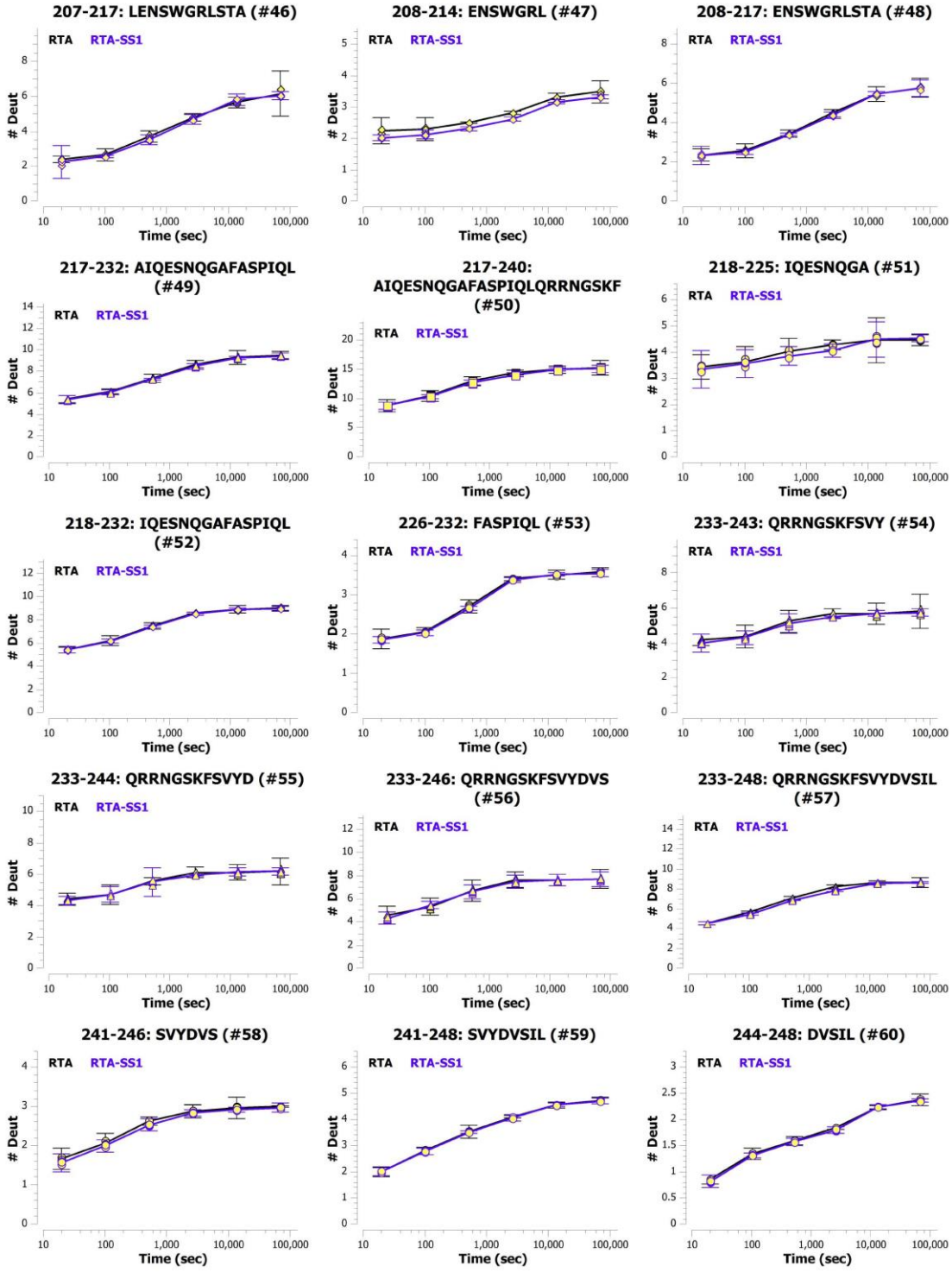
207-217: LENSWGRLSTA (#46)
208-214: ENSWGRL (#47)
208-217: ENSWGRLSTA (#48)
217-232: AIQESNQGAFASPIQL (#49)
217-240: AIQESNQGAFASPIQLQRRNGSKF (#50)
218-225: IQESNQGA (#51)
218-232: IQESNQGAFASPIQL (#52)
226-232: FASPIQL (#53)
233-243: QRRNGSKFSVY (#54)
233-244: QRRNGSKFSVYD (#55)
233-246: QRRNGSKFSVYDVS (#56)
233-248: QRRNGSKFSVYDVSIL (#57)
241-246: SVYDVS (#58)
241-248: SVYDVSIL (#59)
244-248: DVSIL (#60)
RTA
RTA-SS1
Deut
Time (sec)
10
100
1,000
10,000
100,000

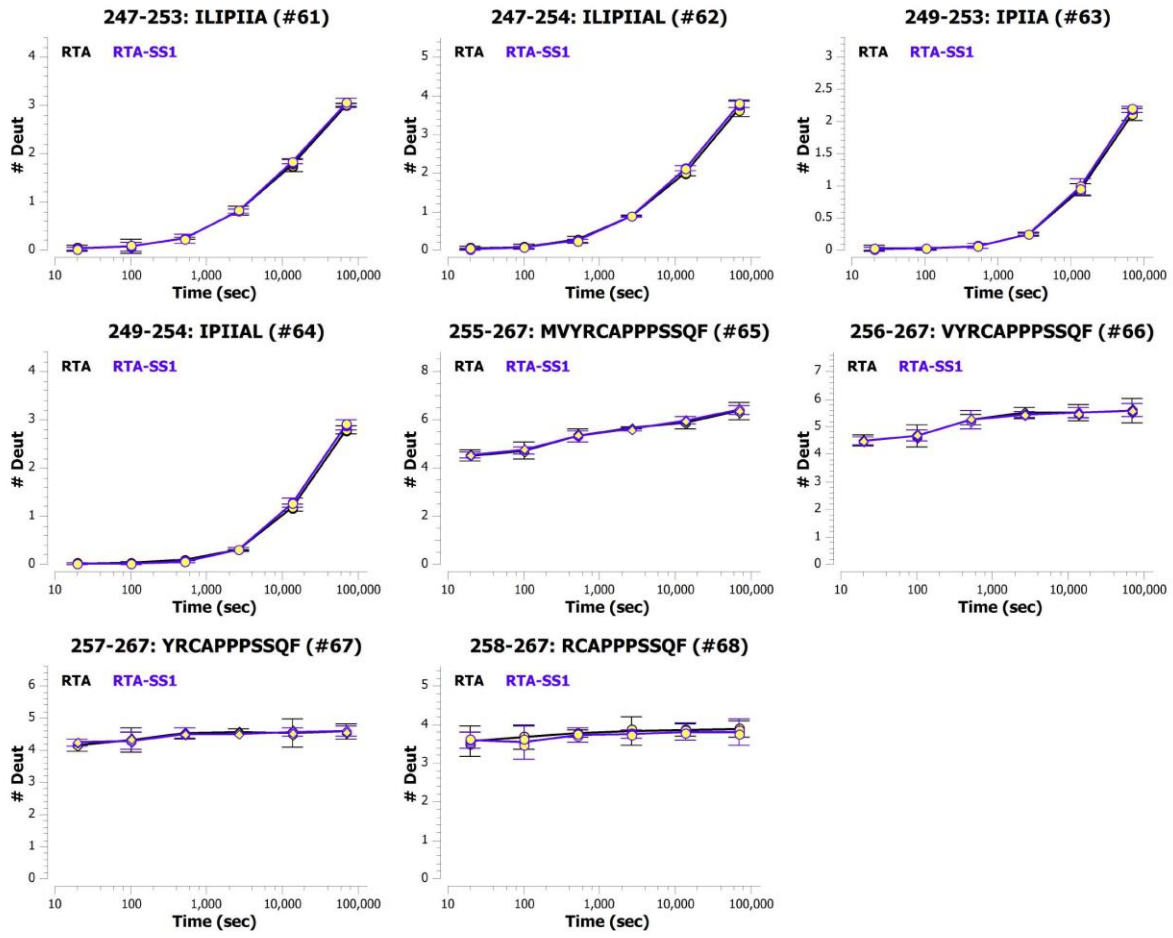

Figure 4.C-2. Deuterium uptake plots for RTA* (black color) and RTA*-SS1 (violet color).